UNIVERSITÀ
DEGLI STUDI
DI PADOVA

UNIVERSITÀ DEGLI STUDI DI PADOVA

DIPARTIMENTO DI INGEGNERIA INDUSTRIALE

CORSO DI LAUREA MAGISTRALE

IN CHEMICAL AND PROCESS ENGINEERING

Tesi di Laurea Magistrale in Chemical and Process Engineering

TECHNO-ECONOMIC ANALYSIS OF A CRYOGENIC CARBON CAPTURE PLANT APPLIED TO CEMENT PRODUCTION

Relatore: Prof. Fabrizio Bezzo
Correlatori: Prof. Federico d'Amore
Ing. Leonardo Varnier

Laureando: RUBINACCIO DAVIDE

ANNO ACCADEMICO 2023-2024

Abstract

The growing concern over climate change has led to increasingly stringent environmental regulations aimed at reducing CO_2 emissions. Although carbon capture technologies currently focus on more established methods, cryogenic techniques offer significant advantages, including high-purity CO_2 products suitable for various industrial applications, the elimination of toxic chemical solvents, and reduced energy consumption. This thesis presents a techno-economic analysis of a cryogenic carbon capture process simulated in Aspen Plus®, applied to flue gases from a cement plant, one of the largest industrial contributors to greenhouse gas emissions. CO_2 is separated from the gas mixture in a desublimation column operating at atmospheric pressure and a temperature of -115 °C, achieving a CO_2 capture rate of 90% with a product purity exceeding 99.99%. Following the simulation, an economic evaluation was conducted to assess both capital and operational costs. These cost assessments form the basis for estimating key performance indicators, including the Avoided CO_2 index, the Cost of Avoided CO_2, and the Specific Primary Energy Consumption for CO_2 Avoided. The results indicate that cryogenic carbon capture is less energy-intensive than conventional methods, with an energy penalty of 1.10 MJ_{el}/kg_{CO2}. This research underscores the potential of cryogenic technology as an advanced and economically feasible solution for CO_2 capture, particularly in high-emission industries such as cement production.

Table of contents

Introduction

The accumulation of greenhouse gases in the atmosphere, particularly carbon dioxide (CO_2), has detrimental effects on human health and to climate change. Reducing CO_2 emissions has become a critical goal for researchers and governments worldwide. Technologies for capturing CO_2, such as pre-combustion, post-combustion, and oxyfuel combustion, offer promising solutions to global warming and climate change.

Process chemistry is the primary CO_2 emitter, accounting for approximately 50% of the overall CO_2 emissions. Cement production is responsible for 6% of global greenhouse gas (GHG) emissions, rendering the sector the second largest industrial emitter after steel. Cement's carbon footprint averages 0.59 ton of CO_2 per ton of cement, which varies due to different production technologies, fuel mixes, efficiency measures and cement types in each region (Ferrario et al., 2023). This implies that the implementation of CO_2-free fuels alone is insufficient to eliminate CO_2 emissions from cement production. Carbon capture, utilization, and storage (CCUS) will play a pivotal role in the efforts to reach a net-zero CO_2 emission path by 2050, as set by the UK, France, New Zealand, and Sweden. A CCUS supply chain (Figure I.1) refers to the series of processes, technologies, and infrastructure required to capture CO_2 emissions from industrial or energy-related sources, transport the captured CO_2 to a location where it can either be utilized in various applications or stored permanently to prevent its release into the atmosphere (IPCC, 2022).

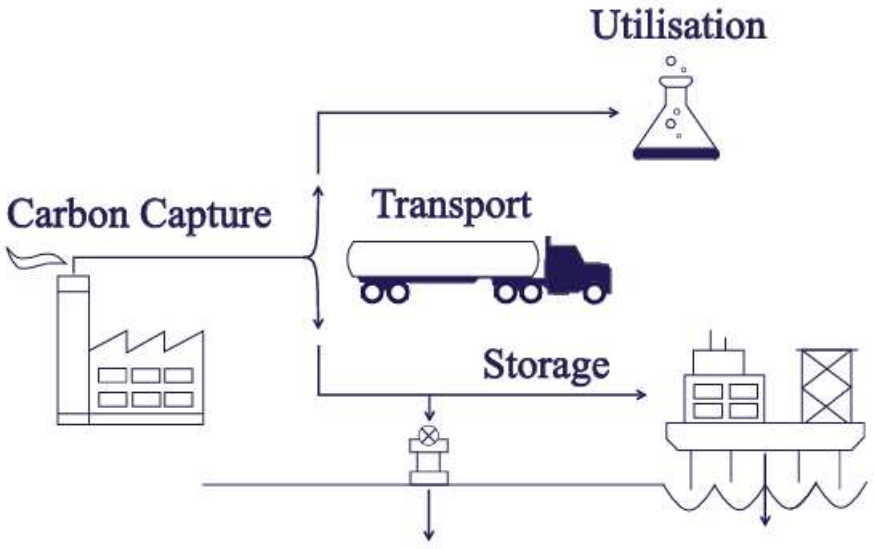

Figure I.1 *Conceptual illustration of carbon capture, utilization and storage supply chain (IEA, 2021).*

The growth of newly announced integrated CCUS units has been rapid since 2017, with the majority of these units located in the United States, Europe, Australia, China, Korea, the Middle

East, and New Zealand. Figure I.2 illustrates the evolution of the number of CCUS facilities from 2010 to 2021. If all projects are launched, the global CO_2 capture potential could increase to approximately 130-150 $MtCO_2$/year, up from the current level of 40 $MtCO_2$/year (as of 2022). This increase is expected to continue, reaching 5.6 Gt by 2050, in an effort to not only decarbonize the power sector but also to reduce emissions in industries such as cement, steel, and chemicals. Stronger climate and investment incentives are driving forces behind the development and implementation of CCUS technology (Madejski et al., 2022).

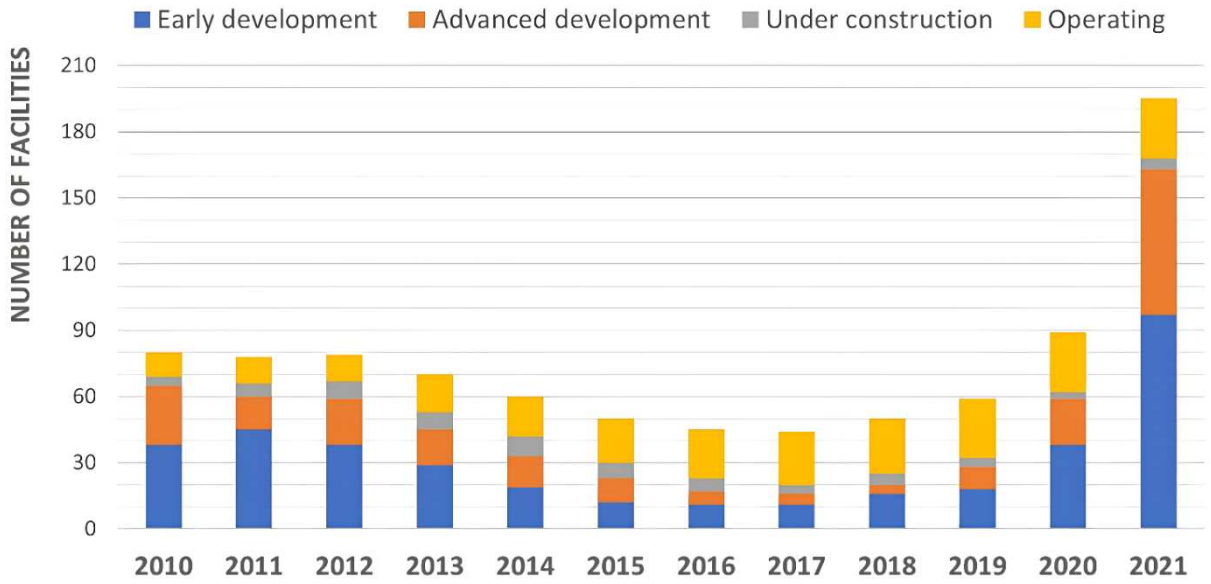

Figure I.2 *Number of CCUS facilities, operating and under development, around the world (Madejski et al., 2022).*

Carbon capture in the cement sector has focused on mature technologies, such as chemical absorption using amine-based solvents, but solvents require significant amount of thermal energy for regeneration. This shortcoming is promoting research on emerging technologies, including low temperature CO_2 capture techniques.

The Cryogenic CO_2 Capture (CCC) process, as a novel post-combustion CO_2 capture technology, is gaining popularity due to its remarkable advantages (Asgharian et al., 2025):

- lower energy consumptions than conventional processes;
- high rates and purity, so it is feasible for both small and large-scale applications;
- as this process relies almost completely on electricity, it does not require chemical solvents;
- high flexibility and easy retrofitting to existing plants.

The CCC process developed by Chart and Sustainable Energy Solution has been recognized by national organizations, as an innovative and industry-disrupting approach to carbon capture. However, this technology has still a low Technology Readiness Level (TRL) and require further development and large-scale demonstrations to increase confidence in the technology.

This work aims at analyzing the techno-economic performance of this technology applied to a cement plant, since the available literature lacks the assessment of the CCC process within the framework of its integration into large-scale chemical plants, particularly in terms of enhancing its efficiency for capturing CO_2 from cement factories. The primary objectives of this thesis are to conduct a comprehensive evaluation of the performance of CCC technology, with a specific focus on its energy consumption and economic impact. This is achieved through a detailed analysis of critical parameters, such as the energy penalty associated with the process and key performance indicators (KPIs), to quantify the efficiency and feasibility of CCC in cement industry. Furthermore, the study aims to compare the simulation outcomes with those of existing carbon capture technologies, highlighting areas of relative strength or weakness in terms of energy efficiency and cost-effectiveness. Through a comprehensive comparison, this research will provide valuable insights into the potential of CCC technology for commercial deployment in cement production. Moreover, it will contribute to a deeper understanding of whether CCC can serve as a viable alternative to existing carbon capture technologies, supporting efforts to achieve global decarbonization targets. This study presents a novel validation of the Peng-Robinson Equation of State (EoS) in Aspen Plus®, combined with the Jäger and Span (2012) EoS for solid CO_2, utilized to simulate the entire CCC process. The validation aims to ensure the reliability of the simulation results, thereby preventing inaccurate predictions or incorrect equipment sizing.

This dissertation begins with a background reviewing various carbon capture technologies, including both more mature techniques and cryogenic ones. Following this background section, the Cryogenic CO_2 capture investigated is described in detail. Chapter 2 discusses the methods developed to assess the technology, including the selection and validation of a suitable thermodynamic model and the modeling of the process units in Aspen Plus. Additionally, it covers the economic analysis, which involves calculating capital, fixed, and operating costs to determine KPIs. The last section is dedicated to the discussion of the results, in terms of the energy and economic indicators such as CO_2 avoided index, specific primary energy consumption per CO_2 avoided (SPECCA) and cost of avoided CO_2. In the end, conclusions summarize the most important findings of this study together with future perspectives.

Chapter 1

Carbon capture

This chapter provides an overview of the cement production process, focusing on the factors that impact on the flue composition leaving the plant. Afterwards, different carbon capture technologies are reviewed, starting from the more mature ones to then examining cryogenic techniques. This serves to compare the advantages and disadvantages of these technologies, to understand the potential benefits in adopting cryogenic CO_2 capture techniques.

1.1 Cement production process

The initial step in cement production is the processing of raw materials, consisting of different minerals such as limestone, clay, sand and iron ore, to obtain the raw meal. The pre-processing comprises crushing, storing, proportioning, and grinding. The raw materials are then transferred to the kiln system, where clinker, the main constituent of cement is produced. In the process, temperatures can reach up to 1450 °C, by means of fossil fuel combustion. In modern cement plants, raw meal passes through a preheater and a pre-calciner before reaching the rotary kiln. These equipment are added to increase the energy efficiency and consequently decrease heat consumption. One of the main reactions in the process is calcination (Equation 1.1), which occurs in the pre-calciner and consists in the decomposition of calcium carbonate ($CaCO_3$) into calcium oxide (CaO) and carbon dioxide (CO_2).

$$CaCO_3 \rightarrow CaO + CO_2 \quad \Delta H_R^0 = 178\ kJ/mol \tag{1.1}$$

The calcined material enters the rotary kiln where the clinker is formed at high temperature. Afterwards, the clinker undergoes a cooling step by heat exchange with an air flow and the final processing where it is mixed with additives to produce the cement. A simplified scheme of the cement production is presented in Figure 1.1.

While the cement production process is simpler than other emission-intensive industries, its decarbonization can be more challenging. The cement manufacturing involves process emissions, namely the ones related to chemical or physical transformation other than fuel combustion. These processes emissions, are associated to the calcination process, and their mitigation can be only achieved via carbon capture technologies. CO_2 emissions are generated in the calcination reactions which account for approximately 50%. The combustion process accounts for approximately 40 % of the CO_2 emission. Finally, the use of electricity and transport constitutes the remaining 10 % of the CO_2 emission (Khaiyum et al., 2023). Flue gas

composition depends mainly on two factors: operation mode of the kiln and the air leak considered in the process.

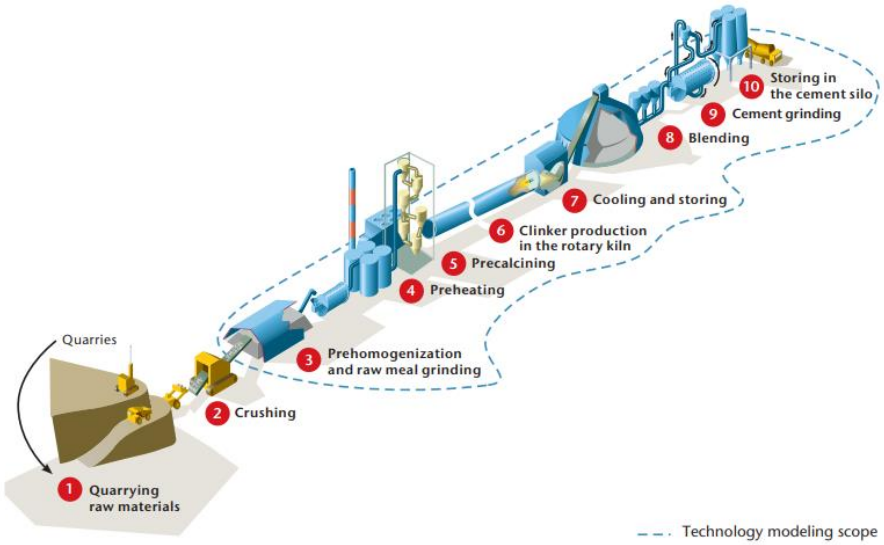

Figure 1.1: *Schematic diagram of the cement production process (IEA, 2018).*

In a cement production plant, the kiln switches between the so-called interconnected and direct mode of operation during the daily operation, and this has an impact on the resulting flue gas characteristics. In the interconnected mode, the flue gas is sent to the raw mill where the thermal energy contained in the flue gas is used to dry the raw materials mix. After the raw mill, the mixture is sent to the filter where the solids are separated from the gas before the gas is sent to the stack. In this mode the kiln and the raw mill are operating in a completely interconnected way, as a single machine, on the other hand, in direct mode, the flue gas bypasses the raw mill and is sent directly to the dust filter. In interconnected mode, CO_2 concentration will be lower since the drying flue gas are more diluted due to the evaporation of humidity within the raw materials. A cement kiln is run in interconnected mode typically 90% of the time during a day (21-22 h/d) as stated in Voldsund et al. (2019).

Table 1.1: *Stream data for the flue gas condition considered in Voldsund et al. (2019).*

		REFERENCE
Property	**Unit**	**Value**
Total flow rate	kg/h	318192
Temperature	°C	130
Pressure	atm	1
Gas composition		
CO_2	% mol	22
N_2	% mol	60
O_2	% mol	7
H_2O	% mol	11

Another important factor that affects the flue gas composition is the air leak in the system, which occurs typically at the kiln inlet and outlet, in the calciner, in the preheating stages, and in the raw mill. Air leaking into the process is referred to as "false air". The amount of air leak also changes a lot during the classical year of operation, it increases over the year and is reduced during maintenance periods. The flue gas conditions, reported by Voldsund et al. (2019), for “low air leak” scenario are described in Table 1.1.

1.2 Post-combustion carbon capture technologies

Carbon capture technologies are divided into three main categories: pre-combustion, oxy-fuel combustion and post-combustion techniques. Pre-combustion carbon capture allows CO_2 to be removed from a gas mixture before combustion occurs. The principle of operation involves the partial oxidation of the fuel into oxygen/air and steam at high temperature and pressure to produce synthetic gas (or syngas). Being a mixture of carbon monoxide, carbon dioxide, hydrogen, and small portions of other gaseous components, such as methane, the syngas can undergo the water-gas shift reaction to produce a gaseous mixture composed significantly of H_2 and CO_2. The concentration of CO_2 in this mixture varies from 15% to 50% (Kanniche et al., 2010). Therefore, pre-combustion carbon capture primarily addresses energy-related emissions, limiting its potential for reducing overall emissions in cement plants.

In oxy-fuel combustion, oxygen is used for combustion instead of air. It produces a flue gas mainly consisting of H_2O and CO_2 and therefore allowing simple CO_2 purification. However, oxygen combustion increases the temperature profile in the kiln which can cause structural damage to the equipment. It is therefore essential that a portion of the CO_2 rich flue gasses are recycled back to the combustion zone to moderate the flame temperature (Gerbelova et al., 2017). Another operational concern of an oxyfuel layout is corrosion from the flue gases in the recycle loop and a capital and energy expansive air separation unit (ASU) to procure the oxygen needed by the combustion process.

The post-combustion CO_2 capture techniques are the most straight-forward ones: they are based on separating carbon dioxide from flue gas at atmospheric pressure by placing the capture unit after other purification systems, such as desulphurization, denitrogenation, and dedusting. Nevertheless, a significant challenge in implementing these methods is the low partial pressure of CO_2 in the flue gas, with concentrations typically ranging between 13% and 15% in conventional power plants. Thus, the driving force for CO_2 is also low, leading to lower performance and higher gas volumes to be treated, so larger equipment size (Olajire, 2010). Flue gas from cement plants have higher concentrations, as previously shown in Table 1.1.

1.2.1 Chemical absorption

Chemical absorption is the most recognizable method of CO_2 capture. It relies on the reaction between carbon dioxide and a chemical solvent. Solvents that are usually employed are alkanolamines, such as monoethanolamine (MEA), diethanolamine (DEA), or methyl diethanolamine (MDEA) in aqueous solution. The flue gas reacts with the solvent in the absorber capturing CO_2. Subsequently, the rich loading solution is carried to the stripper regenerating the solvent at elevated temperatures and releasing pure CO_2, then the regenerated solvent (lean-loading solution) is recycled back to the absorber column. The high purity carbon dioxide is sent to compression before being transported to storage or utilization.

The energy penalty of the process, namely the increase in plant electricity input per unit of CO_2 captured, ranges from 0.72-4.20 MJ_{el}/kg_{CO2} depending on the flue gas source and the design of the system. Generally, an amine carbon capture system applied to cement plants has an energy penalty of about 1.3 MJ_{el}/kg_{CO2} captured (Wang et al., 2024). The primary disadvantages of chemical absorption are the significant energy required to operate the system, the amount, toxicity, and chemical instability of the solvent, the cost, and the incompatibility of the technology with traditional power plant operations in terms of load following, operation, and design. The principal energy demands are associated to steam generation required for solvent regeneration, in fact the thermal energy penalty associated to this operation is in the range 3.7-4.4 MJ_{th}/kg_{CO2} for cement plant flue gas (Font-Palma et al., 2021).

A schematic diagram of chemical absorption in shown in Figure 1.2.

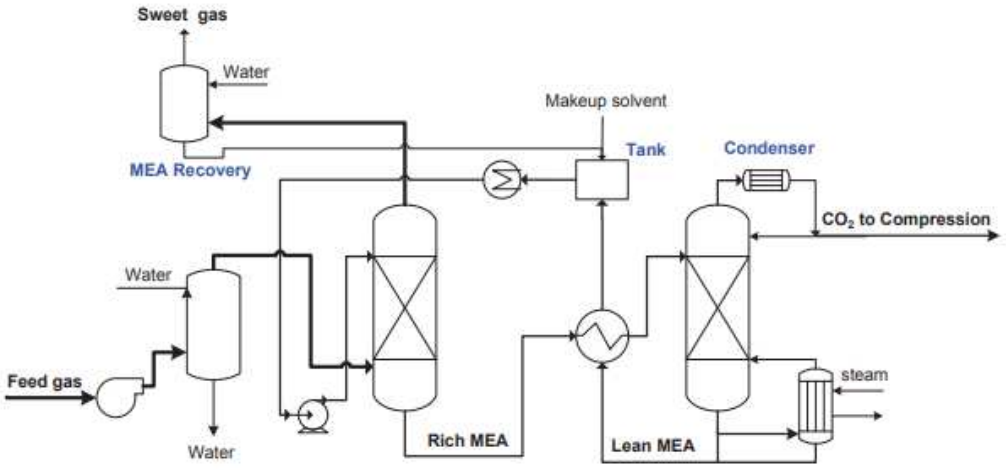

Figure 1.2: *Scheme of the amine absorption CO_2 capture process (Husebye et al., 2012).*

1.2.2 Physical adsorption

Physical adsorption uses the affinity of CO_2 to material surfaces. It relies on the weak van der Waals forces and no chemical bonds are formed. In this way, CO_2 can be selectively separated by solid adsorbents from a stream of gases at a high pressure. The chemical potential in the solid phase of CO_2 is higher when compared to the gas phase, and the adsorbent materials are capable of reversing the chemical potential of the solute gas component in the solid phase to release CO_2 (Zaman, 2013).

Adsorption depends on the operating temperature and pressure, surface forces, and adsorbent pore size. Adsorption capacity increases with higher partial pressure of CO_2 and lower temperature. Low energy requirements and low time for regeneration, as it can be done with pressure swings, are the main advantages of physical adsorption (Zaman, 2013). On the other hand, high selectivity materials for CO_2/N_2 are required. In addition, most physical adsorbents favor H_2O adsorption over CO_2, and therefore, flue gas must be dried.

One application of physical adsorption is the vacuum pressure swing adsorption which is a widely-used technology for gas separation that is employed in various applications, and so has a high Technology Readiness Level (TRL). Swing Adsorption Reactor Cluster (SARC) is a new post-combustion capture concept utilizing only electricity to capture CO_2. The process is reported in Figure 1.3 and consists in fluidized bed reactors cycling through four process steps:

1. Carbonation, where a sorbent adsorbs CO_2 from the cement plant flue gas stream.
2. Evacuation, where N_2 is extracted from the reactor and vented to the atmosphere to prevent it from diluting the CO_2 released in the subsequent regeneration step.
3. Regeneration, where the sorbent is regenerated using a combination of temperature increase and pressure decrease.
4. Cooling, where the bed is cooled and repressurized in preparation for the subsequent carbonation step.

The estimated energy penalty for this process is 1.15 MJ_{el}/kg_{CO2} with a 90% of carbon capture (Cloete et al., 2020) that is lower than traditional CO_2 capture technologies. However, the disadvantage of this technique is that the purity of captured CO_2 can be up to 96%, requiring further treatments to be utilized in other industrial applications, this will rise the energy consumptions.

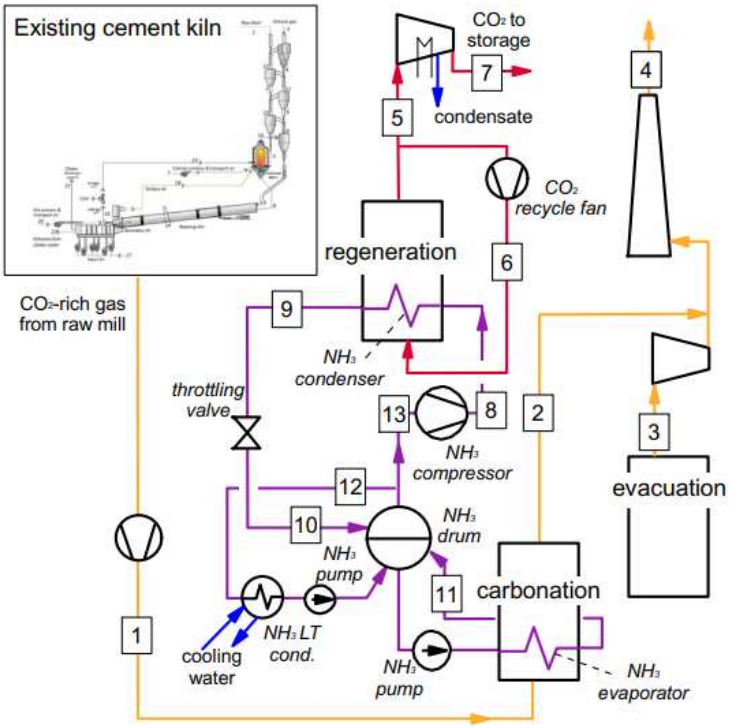

Figure 1.3: *Schematic of the proposed integration of the SARC process in a cement plant (Cloete et al., 2020).*

1.2.3 Membranes

Membranes are increasingly being used in post-combustion carbon capture processes as an alternative to chemicals. Membranes are commonly made of polymers that allow CO_2 permeate selectively with respect to other gases, such as N_2. In the conventional case, the membrane separates gas into two streams: the stream rich in CO_2 is called permeate, while the clean gas stream is called retentate. The partial pressure difference of the species across the membrane is the driving force, and this driving force can be generated by pressurizing the gas stream on the retentate side.

Membrane process is a less mature technology than amine processes. The main advantage of membranes is that they do not use toxic chemicals, but requires frequent replacement of membranes and significant pumping power, resulting in energy penalties ranging from 0.95 to 1.9 MJ_{el}/kg_{CO2} (Scholes et al., 2014).

In the study of Lindqvist et al. (2014) a membrane separation process is modelled with a cement plant flue gas feed. The results show that a single stage design can achieve only 95% of CO_2 purity and requires a massive feed compression and membrane area, leading to prohibitively large separation costs, for this reason multi-stage designs are usually employed. Three-stages design does not offer a good trade-off between fixed and operative costs and CO_2 purity, a two-

stages design seems the best option to obtain a trade-off between CO_2 purity and operation costs. Figure 1.4 shows a schematic diagram of a CO_2 two-stages membrane separation process.

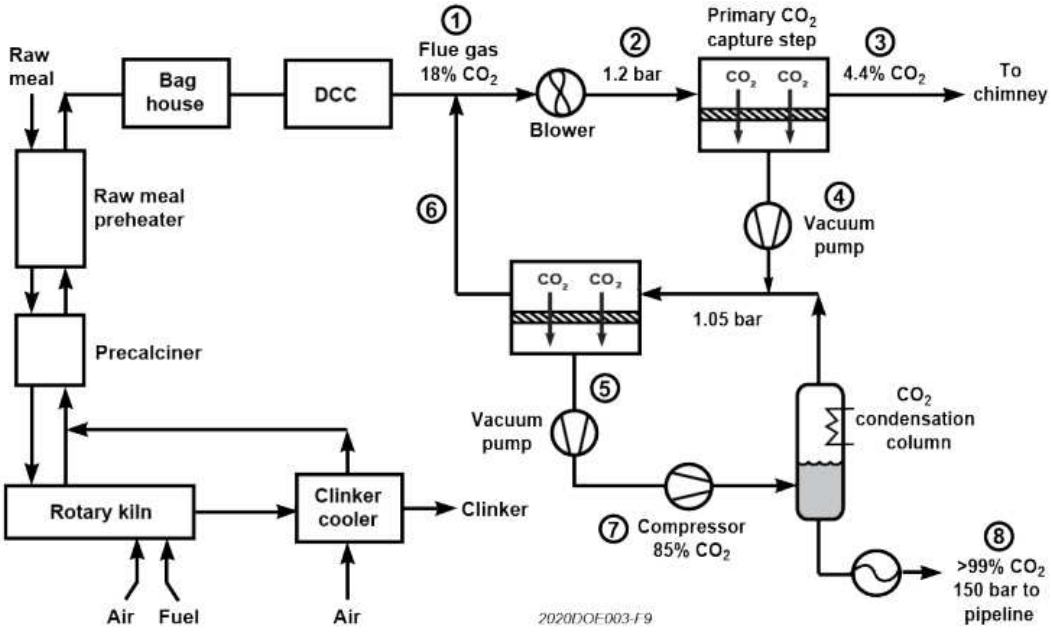

Figure 1.4: *Scheme of the post-combustion CO_2 capture method using two membranes (NETL, 2020).*

1.2.4 Calcium Looping

The concept of "calcium looping", or "carbonate looping", embraces a wide variety of CO_2 capture process routes with different levels of maturity, technical complexity and economic viability. All these process options share the use of calcium oxide as a regenerable sorbent of CO_2.

Flue gas containing CO_2 from a cement plant are put in contact with a solid stream containing CaO in a carbonator reactor operating at about 650 °C, where the exothermic carbonation reaction occurs (Equation 1.2). Solids containing the $CaCO_3$ formed by the carbonation reaction are sent to a calciner for regeneration, to calcine the $CaCO_3$ formed in the previous step at a temperature of 900–950 °C. The high temperature needed in this reactor for the endothermic calcination of $CaCO_3$ (Equation 1.1) under high CO_2 partial pressures is achieved by burning additional fuel in the reactor with oxygen to avoid dilution of the pure CO_2 stream formed (Abanades et al., 2015).

$$CaO + CO_2 \rightarrow CaCO_3 \quad \Delta H_R^0 = -178\ kJ/mol \tag{1.2}$$

One of the inherent advantages of this technology is that most of the fuel chemical energy introduced into the calciner can be recovered as high temperature heat in the process and potentially converted into electricity with high efficiency. Moreover, the CaO-based sorbent derives from natural sources (i.e., limestone), which is characterized by low cost and wide availability and it is the main raw material of cement production. One drawback of the process is the need of a continuous make-up of fresh limestone to compensate the purge of solids from the Calcium-Looping (CaL) loop to avoid build-up of coal ash and $CaSO_4$ originating from coal combustion in the calciner. Additionally, it is needed to keep a proper activity of the sorbent, which reduces with the number of carbonation-calcination cycles. On this regard, the integration of the CaL process in a cement plant provides synergies because the amount of limestone needed for clinker production largely exceeds the make-up need of the CaL process and the CaO-rich purge can be conveniently used in the cement kiln for clinker production. A conceptual scheme of the process is provided in Figure 1.5.

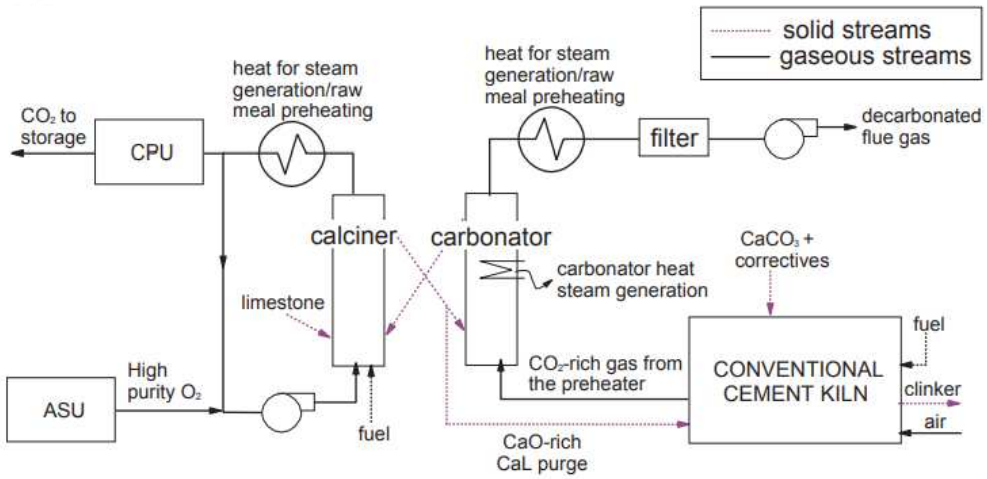

Figure 1.5: *Scheme for the integration of a CaL process into a cement plant (De Lena et al., 2019).*

The CaL process can reduce direct CO_2 emissions from cement kilns by more than 90%, obtaining in the end CO_2 with a purity of about 96%, so a further purification may be needed for CO_2 transport and utilization. Additionally, this process requires intrinsically high fuel consumptions: between twice to three times larger than a reference cement kiln without CO_2 capture, leading to a SPECCA (Specific Primary Energy Consumption for CO_2 Avoided), ranging from 3.49 to 3.60 MJ_{LHV}/kg_{CO2} (De Lena et al., 2019). This index quantifies the increased equivalent fuel consumption to avoid the emission of CO_2 in a cement kiln with CO_2 capture with respect to a reference cement kiln without capture.

1.3 Cryogenic carbon capture

Gaseous CO_2 can be separated from other components in the flue gas due to their different condensation and desublimation temperatures. These methods are gaining more popularity because are capable to capture CO_2 with higher rates and purities, with a low energy demand. Moreover, other studies such as the one of Baxter et al., (2021) have indicated that CO_2 capture costs can be decreased by 20–40% when the Cryogenic Carbon Capture (CCC) process is used, and it distinctly indicates the economic advantages of the CCC process over other methods. Furthermore, this technology can be easily installed at the current industrial emission facilities without any concern regarding chemical solvents or physical sorbents.

Despite all benefits and advantages of the CCC processes, this technology is still in its early stages of development and deals with several challenges such as ice plugging when the flue gas is not water-free. Moreover, this technology can be uneconomical when the CO_2 mole fraction in the gas mixture is very low. Techno-economic evaluations have indicated that for large-scale applications, the CCC process costs are comparable with mature conventional MEA absorption technology, while in smaller scales, the costs are significantly lower in the case of using the CCC process rather than MEA (Asgharian et al., 2025).

1.3.1 Cryogenic distillation

Distillation is one of the most employed separation technologies, it exploits the difference in boiling temperatures to separate the components through vapor-liquid equilibria.

The cooled feed gas is sent to the distillation column, which contains a number of vapor-liquid contact devices (such as trays or packing materials) and separates the CO_2 from the off-gases. Condensed CO_2 is collected at the bottom of the distillation column, where part of the CO_2-rich stream is vaporized in a reboiler and recycled to the distillation column. The other part of the CO_2 stream is further separated from the alkanes mixture and finally, the purified CO_2 product is extracted from the separator (Song et al., 2018). This process is highly energy-intensive because the off-gas must be compressed before entering the distillation column to increase the pressure above the CO_2 triple point and prevent dry ice formation. Maintaining the pressure above the CO_2 triple point ensures a gas-liquid transition rather than a gas-solid transition (Aaron and Tsouris, 2005). However, cryogenic distillation has several advantages. It can achieve a recovery rate, namely the ratio between CO_2 captured and CO_2 fed to the process, of over 99% and a CO_2 purity above 99.5 mol%. Furthermore, the estimated energy penalty for the cryogenic distillation process is relatively low at 1.47 MJ_{el}/kg of captured CO_2, compared to other conventional technologies (Song et al., 2018). A conceptual scheme of the process is presented in Figure 1.6.

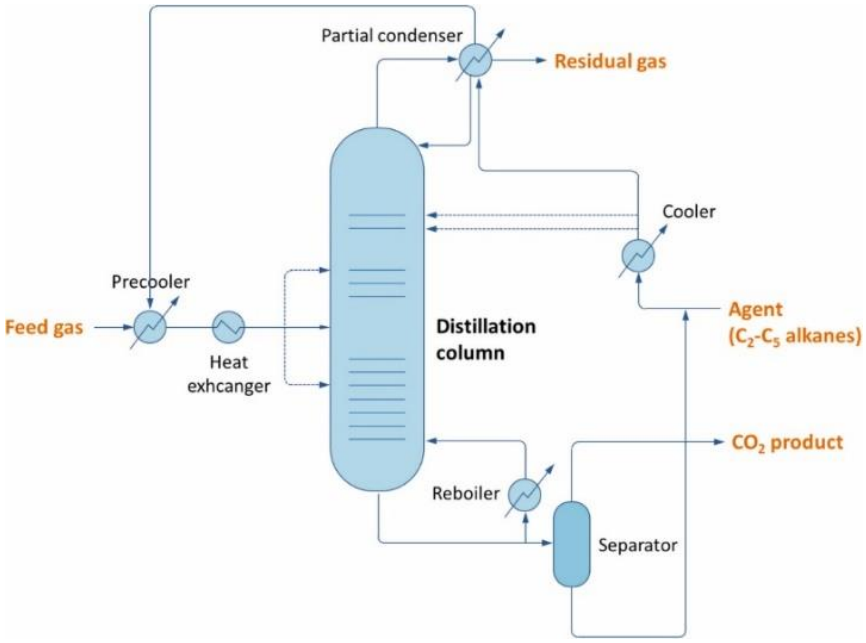

Figure 1.6: *Schematic diagram of cryogenic distillation (Song et al., 2018).*

1.3.2 Cryogenic solid-vapor separation

Cryogenic solid-vapor separation is based on the separation of the CO_2 from flue gases in solid phase and has demonstrated promising results. The main step of the process is the dry-ice formation, which occurs inside the desublimation column by means of a contact liquid, specifically a hydrocarbon with low vapor pressure. The desublimation of CO_2 in the bulk of the contact liquid prevents solid formation on the column walls that worsens the heat exchange and may ruin the equipment material. To achieve the vapor-solid transition, it is important to operate at pressure lower than the CO_2 triple point (5.18 bar). This technology can achieve a recovery rate and a CO_2 purity larger than 99% and 99,99% respectively, depending on the operating temperature of the desublimation column. This indicates that this process can meet CO_2 purity requirements without additional treatments.

Researches had shown that CCC is capable to obtain an energy consumption for the carbon capture lower than 1 MJ_{el}/kg of captured CO_2. Compared to other techniques that utilize solvents or air separation units, CCC offers 30-50% reduction in overall energy consumption (Asgharian et al., 2025).

Baxter et al. (2021) demonstrated that the CCC technique could capture CO_2 from coal-fired power plants with an energy penalty of 0.894 MJ/kg_{CO2}, a significantly lower value than that of other technologies. Willson et al. (2019) compared the CCC process with conventional amine-based methods across various applications, including oil-fired boilers, biogas upgrading, and combined gas turbines. Their study highlighted the CCC process's feasibility for a wide range

of CO_2 concentrations in flue gases, suggesting economic advantages over amine-based processes, particularly in smaller-scale operations. Song et al. explored a CCC process using Stirling coolers to desublimate and separate CO_2 from flue gas, achieving a 96% CO_2 capture efficiency with an energy penalty of 1.5 MJ/kg_{CO2}. Jensen et al. (2015) assessed the CCC process's performance for CO_2 capture from a 550 MW coal-fired power plant, employing bench-scale experiments and Aspen Plus simulations. Their findings indicate that the energy penalty of the CCC process ranges between 0.71 and 0.92 MJ/kg_{CO2}. Asgharian et al. (2025) investigated the integration of the CCC process with a water-ammonia Absorption Refrigeration Cycle (ARC) for CO_2 capture from cement factory flue gas, achieving an energy penalty below 0.7 MJ/kg_{CO2}.

The most recent field testing of CCC technology occurred in 2018 at the Argos Cement Plant in Alabama, US, and later at the PacifiCorp Hunter Plant in Utah, US. At the Argos plant, the CCC process successfully captured and liquified the CO_2, reducing its concentration in the clean gas stream to below 0.5%. This marked the first practical demonstration of CCC technology in a cement plant. Afterward, the system was relocated to the PacifiCorp Hunter power plant, where it operated for nine months. During this period, it consistently maintained low CO_2 concentrations in the clean flue gas, ranging from 0.3% to 1.3%, despite inlet CO_2 concentrations fluctuating between 7.1% and 14.9% (Frankman et al., 2021).

Despite growing interest in this technology, further research is required to advance its TRL, particularly in cement sector applications.

The process scheme of CCC, developed by Chart and SES (Chart Industries Inc, 2019) and central to this study, is provided in Figure 1.7. Initially, the off-gas is dried to lower the water content and sent to the desublimation column at temperatures around -100 °C, the temperature is chosen based on the CO_2 concentration in the flue gas, to avoid dry-ice formation upstream the desublimation column. The flue gas is cooled to those temperatures by exchanging heat with the CO_2-poor gas exiting the process. Within this unit, CO_2 is separated from the non-condensable gases through desublimation, achieved by further cooling provided by the contact liquid. It is important to note that the CO_2 recovery depends mainly on the temperature of the contact liquid. The slurry of contact liquid and solid CO_2 leaving the desublimation column enters a solid-liquid separator, which could be either hydrocyclones or decanter centrifuges (disc or screw), to increase the mass fraction of CO_2 in the process stream. The solid CO_2 is then melted in the multi-stream heat exchanger before undergoing a final purification in a distillation column. In this step, the remaining amount of contact liquid is separated to achieve a CO_2 concentration that meets the purity requirements for transportation and storage (Baxter et al, 2021).

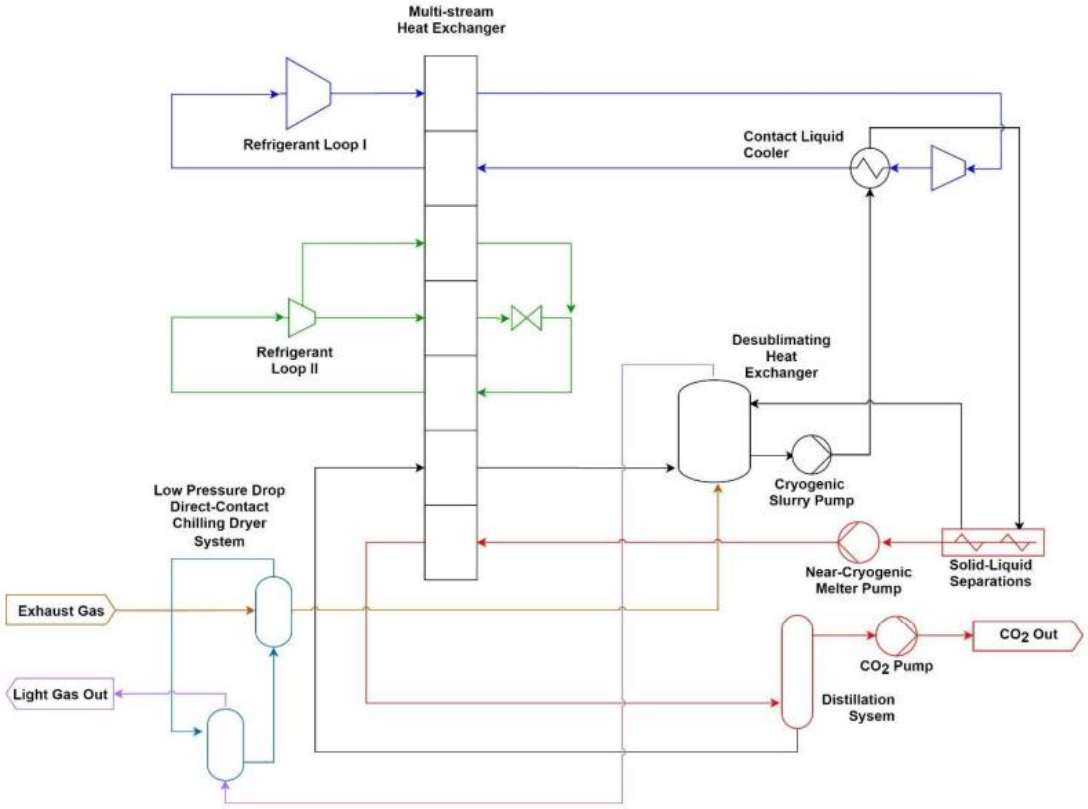

Figure 1.7: *Flow diagram of solid-vapor separation process, Baxter et al. (2021).*

After the condenser of the distillation column, the CO_2 is collected in liquid phase, avoiding the need of an energy- and capital-intensive gas compression section to meet the pressure specification for CO_2 transportation, a centrifugal pump is sufficient to compress CO_2 up to 110 bar. This is a significant advantage of this technology with respect to amine separation or VPSA. Another significant benefit is that this process uses only electrical power, except for heat provided by steam in the distillation column reboiler.

1.4 Overview of separation technologies

Amine absorption and VPSA are currently the most widely used technologies, but the cryogenic methods have some favorable advantages, which could be desirable for carbon capture solutions. Consequently, the most important advantages, disadvantages and a comparison of energy duties of the presented technologies are presented in Table 1.2.

Table 1.2: *Summary of advantages, drawbacks and energy penalty for different CO_2 capture techniques.*

Pros	Cons	Energy Penalty [$MJ/kg_{CO2,\ capt}$]	
		Electrical	**Thermal**
Amine absorption			
• Very mature technique • Most solvents are cheap and suitable for high T operations	• Toxicity, instability, reactivity of solvents • Significant energy required by scrubbing system	1.38	3.7-4.4
Physical adsorption			
• Does not require thermal energy • Very mature technique	• Pre-treatment required for sulfur-based compounds • Low CO_2 recovery and purity	1.15	-
Membranes			
• High purity and recovery of CO_2 • Low operating costs	• High capital investment for large scale operations • Low CO_2 selectivity and purity	1.29	-
Calcium Looping			
• Low cost and availability of sorbents • Low energy penalty	• Low CO_2 purity • High fuel consumption	0.40	2.7
Cryogenic distillation			
• High CO_2 purity • Very mature and validated technique	• High investment costs • Very energy intensive process	1.47	-
Cryogenic solid-vapor separation			
• High recovery and purity of CO_2 • Low energy consumption	• High investment costs • Low TRL	0.85	-

Table 1.2 shows that the VPSA, membranes and calcium looping technologies require further treatments to comply with the CO_2 purity for transportation and storage, which will be very energy consuming. The disadvantage of the amine absorption technology is the excess heat from the regeneration procedure, if this heat cannot be utilized, amine process is very energy-consuming. Alternatively, the cryogenic solutions can achieve a CO_2 purity of > 99.5 %, and thus comply with the desired CO_2 purity requirement. Furthermore, the outlet carbon dioxide product is liquefied, which is very favorable for storage or transportation before the utilization in others industrial sectors. The disadvantages of the cryogenic solutions are the low TRL as well as high capital expenses.

The energy penalty, by definition, considers only electrical energy consumption, while processes as chemical absorption and chemical looping require also a certain amount of thermal energy. Cryogenic distillation and solid-vapor separation require thermal energy in the reboiler of the distillation column, however in a much smaller magnitude compared to the electrical consumptions.
Thus, the thermal energy demand, for cement plant applications, is estimated as 2.7 MJ_{th}/kg_{CO2} for calcium-looping technology (Vatapolous and Tzimas, 2012) and 3.7-4.4 MJ_{th}/kg_{CO2} for amine absorption (Kuramochi et al., 2012).
To summarize what stated before, the main advantages of cryogenic solutions are the capability of achieving very high purities, without the need of further treatments and that the CO_2 product is already in liquid phase. The disadvantages of cryogenic solutions are the high capital expenses and the low TRL.
Cryogenic solid-vapor separation, among cryogenic technologies, has a significantly lower energy consumption. Lastly, this technique seems one of the most suitable for the application in the cement sector and it will be further analyzed in this dissertation.

1.5 Motivations and objectives of the thesis

The implementation of Carbon Capture Utilization and Storage (CCUS) technologies is expected to play a crucial role in addressing the decarbonization of CO_2 emissions, and in particular the focus is on the cement industry being this considered as a hard-to-abate sector due to its significant level of process-related CO_2 emissions.
Capture technologies, presented in this chapter involve a number of drawbacks as low CO_2 purity, high energy penalties and environmental and safety concerns. Cryogenic processes seem capable to overcome these issues, thanks to their potentially higher energy efficiency, significant level of retrofittability in existing plants and to the capability of designing the plant for achieving high-purity CO_2 outlet streams.
The aim of this thesis is to propose a techno-economic study of a cryogenic solid-vapor separation process to capture the CO_2 from cement plant flue gases. Given the limited number of studies on CCC applied to cement plants, this research is particularly relevant. It seeks to demonstrate the viability and effectiveness of this technique, ultimately building confidence in its potential and driving its promoting adoption. The primary objective is to assess the process performance in terms of technical and economic key performance indicators (KPIs), to benchmark its competitiveness against the most widely used CO_2 capture methods.
The baseline process simulation is followed by the sensitivity analyses performed on the main process variables to enhance design and performance. In particular the focus is on determining a suitable operative pressure for the distillation column, and reducing energy consumption in

the most energy-intensive sections of the process, such as the refrigerant loops. Additionally, the thesis validates the application of the Peng-Robinson equation of state to compute CO_2 solid-vapor equilibrium and explores the potential of using alternative contact liquids, evaluating their impact on both the economics and energy requirements for achieving a comparable CO_2 capture rate.

Chapter 2

Methods

This chapter presents the methodologies applied in this study, starting with the validation of the thermodynamic model used for process simulation. Following this, a description of the CCC process simulated in the study is provided, with an emphasis on the analysis of its key operational units. Sensitivity analyses are then performed to determine the optimal operating conditions, as well as the selection of refrigerants and contact liquids. Finally, an economic model is developed to estimate both capital and operating costs, and to establish key performance indicators (KPIs) for evaluating and comparing the CCC process against alternative carbon capture technologies.

2.1 Thermodynamic framework of CCC

Cryogenic solid-vapor separation technology relies on the fact that CO_2 can be separated from the flue gas by freezing it out. As a consequence, when dealing with the design of these type of processes, it is of paramount importance to be able to satisfactorily predict the thermodynamic behavior of the system, which involves equilibrium conditions also in the presence of solid CO_2.

2.1.1 Thermodynamic models for solid-vapor equilibrium

The classical approach for solid-vapor equilibria (SVE) calculations is based on the equality of components' fugacities in the different phases (Equation 2.1), assuming the vapor phase to be a gas mixture and the solid phase to consist of pure CO_2. The fugacity of the component in the solid phase, $\hat{f}_i^S$, can be expressed by relating it to its fugacity in the vapor phase, $\hat{f}_i^V$ (De Guido et al., 2020).

$$\hat{f}_i^S\left(T, P, \underline{x}^S\right) = \hat{f}_i^V\left(T, P, \underline{x}^V\right) \tag{2.1}$$

Since CO_2 is the only species to be present in both phases at equilibrium, this expression can be rewritten as Equation 2.2, where ϕ_{CO2}^V is the fugacity coefficient of pure CO_2 in the vapor phase [-] evaluated at the sublimation pressure P_{CO2}^{subl} [Pa] and equilibrium temperature T [K]. $\hat{\phi}_{CO2}^V$ is the fugacity coefficient of CO_2 in the vapor mixture [-] evaluated at T, at the given

pressure P, and composition $\underline{x}^V$. v_{CO2}^S is the CO_2 solid molar volume assumed to be constant and equal to 0.0282 $m^3/kmol$ (De Guido et al., 2020).

$$\phi_{CO2}^V\left(T, P_{CO2}^{subl}(T)\right) \cdot P_{CO2}^{subl}(T) \cdot exp\left(\frac{v_{CO2}^S \cdot \left(P - P_{CO2}^{subl}(T)\right)}{RT}\right) = P \cdot x_{CO2}^V \cdot \hat{\phi}_{CO2}^V\left(T, P, \underline{x}^V\right) \quad (2.2)$$

The sublimation pressure can be computed, as function of temperature, using the Equation 2.3 proposed by Jensen et al. (2015), which provides results in agreement with literature data in the temperature range 69-217 K. This temperature range is compatible with this study, since the sublimation of CO_2 occurs between 143 K and 163 K in the desublimation column.

$$P_{CO2}^{subl}(T) = exp\left(57.52 - \frac{3992.84}{T} - 4.9003 \cdot \ln(T) 2.415 \cdot 10^{-15} T^6 + \frac{8125.6}{T^2}\right) \quad (2.3)$$

The two fugacity coefficients are calculated using and Equation of State (EoS), therefore the choice of an appropriate thermodynamic model is essential to simulate the CCC process.
Soave-Redlich-Kwong (SRK) EoS, Predictive Soave-Redlich-Kwong (PSRK) EoS, Raoult's law, and Peng-Robinson (PR) EoS can be employed to estimate the solid–vapor equilibrium temperature. Raoult's law is simpler than Predictive Soave-Redlich-Kwong EoS, Soave-Redlich-Kwong EoS, and Peng-Robinson EoS, while it exhibits acceptable accuracy at low pressures; however, it has been demonstrated that it is not suitable for predicting the CO_2 frost point at high pressures (Jensen et al., 2015). They demonstrated that both Peng-Robinson and Soave-Redlich-Kwong EoS accurately predict the CO_2 frost point, with a maximum deviation of 3K observed in most cases. Additionally, Yang et al. (2015) confirmed that PR EoS has higher accuracy in SVE calculations. Therefore, this EoS is adopted in this thesis as thermodynamic model and its accuracy in predicting solid CO_2 properties will be examined in the following paragraph.

2.1.2 Validation of Peng-Robinson Equation of State

To assess the prediction performance of PR EoS, the thermodynamic properties of pure solid CO_2 are calculated in Aspen Plus® V14 and compared with those obtained using the EoS for solid CO_2 proposed by Jäger and Span (2012) (JS EoS), reported in Equation 2.4. This EoS, which is expressed in terms of Gibbs free energy, g, is valid within the range of $0MPa - 500MPa\ and\ 80K - 300K$. Within this range, most of the thermodynamic properties calculated with this EoS are properly represented within the uncertainty of the experimental data, making it a suitable reference for the comparison.

$$\frac{g}{RT_0} = g_0 + g_1\Delta\theta + g_2\Delta\theta^2 + g_3\left\{\ln\left(\frac{\theta^2 + {g_4}^2}{1 + {g_4}^2}\right) - \frac{2\theta}{g_4}\left[arctan\left(\frac{\theta}{g_4}\right) - arctan\left(\frac{1}{g_4}\right)\right]\right\}$$
$$+ g_5\left\{\ln\left(\frac{\theta^2 + {g_6}^2}{1 + {g_6}^2}\right) - \frac{2\theta}{g_6}\left[arctan\left(\frac{\theta}{g_6}\right) - arctan\left(\frac{1}{g_6}\right)\right]\right\}$$
$$+ g_7\Delta\pi\left[e^{f_a(\theta)} + K(\theta)g_8\right]$$
$$+ g_9K(\theta)\left[(\pi + g_{10})^{\frac{n-1}{n}} - (1 + g_{10})^{\frac{n-1}{n}}\right] \quad (2.4)$$

θ and π are respectively the reduced temperature and pressure, $T_0 = 150K$ and $p_0 = 1\ atm$ are model constants, $\Delta\theta = \theta - 1\ and\ \Delta\pi = \pi - 1$, g_i are dimensionless constants, n=7 and $f_a(\theta)$ is given by Equation 2.5, in which g_i^a are dimensionless constants.

$$f_a(\theta) = g_0^a(\theta^2 - 1)$$
$$+ g_1^a \ln\left(\frac{\theta^2 - g_2^a\theta + g_3^a}{1 - g_2^a + g_3^a}\right)$$
$$+ g_4^a \ln\left(\frac{\theta^2 + g_2^a\theta + g_3^a}{1 + g_2^a + g_3^a}\right) + g_5^a\left[arctan\left(\frac{\theta - g_6^a}{g_7^a}\right) - arctan\left(\frac{1 - g_6^a}{g_7^a}\right)\right]$$
$$+ g_8^a\left[arctan\left(\frac{\theta + g_6^a}{g_7^a}\right) - arctan\left(\frac{1 + g_6^a}{g_7^a}\right)\right] \quad (2.5)$$

Due to the limited availability of experimental data for solid CO_2, the underlying assumption for this EoS, is that the pressure dependence of the isobaric heat capacity, thermal expansion coefficient, and compressibility coefficient are negligible within the pressure ranging from 0 MPa and the CO_2 triple point pressure. Equation 2.4 allow for the computation of all thermodynamic properties of the solid CO_2 through its partial derivatives, as detailed in Table 2.1.

Table 2.1: *Relation between thermodynamic properties and Equation 2.4 (Jäger and Span, 2012).*

Thermodynamic Property	Relation with g
Volume	$v = \frac{\partial g}{\partial p}\Big\vert_T$
Entropy	$s = -\frac{\partial g}{\partial T}\Big\vert_p$
Enthalpy	$h = g - T\frac{\partial g}{\partial T}\Big\vert_p$
Internal energy	$u = g - T\frac{\partial g}{\partial T}\Big\vert_p - p\frac{\partial g}{\partial p}\Big\vert_T$
Helmholtz energy	$f = g - p\frac{\partial g}{\partial p}\Big\vert_T$
Isobaric heat capacity	$c_p = -T\frac{\partial^2 g}{\partial T^2}\Big\vert_p$
Cubic expansion coefficient	$\alpha = \frac{\left(\frac{\partial^2 g}{\partial T \partial p}\right)}{\left(\frac{\partial g}{\partial p}\Big\vert_T\right)}$
Isothermal compressibility	$\kappa = -\frac{\left(\frac{\partial^2 g}{\partial p^2}\Big\vert_T\right)}{\left(\frac{\partial g}{\partial p}\Big\vert_T\right)}$

c_p, v, h, g and u have been calculated using both the expressions in Table 2.1 and with Peng-Robinson EoS in Aspen Plus®. The results are compared through parity plots (Figure 2.1-2.5), to assess the accuracy of the values computed by the process simulator. The range of temperatures considered is from 123.15 K to 193.15 K, as this interval is relevant for the cryogenic carbon capture process

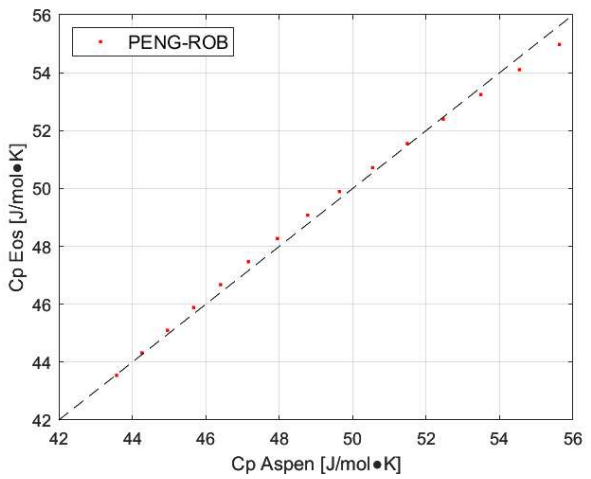

Figure 2.1: *parity plot of c_p.*

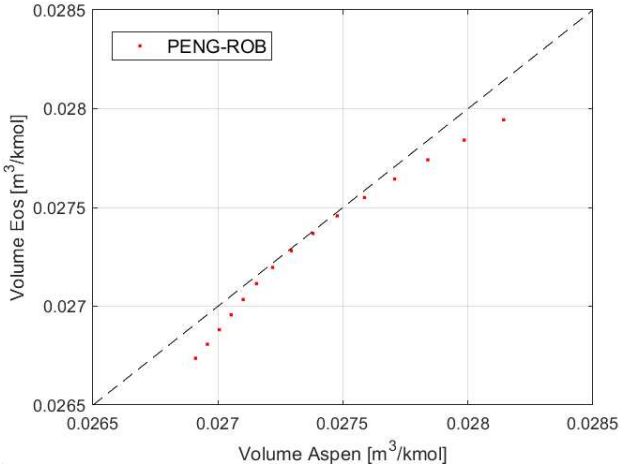

Figure 2.2: *parity plot of molar volume.*

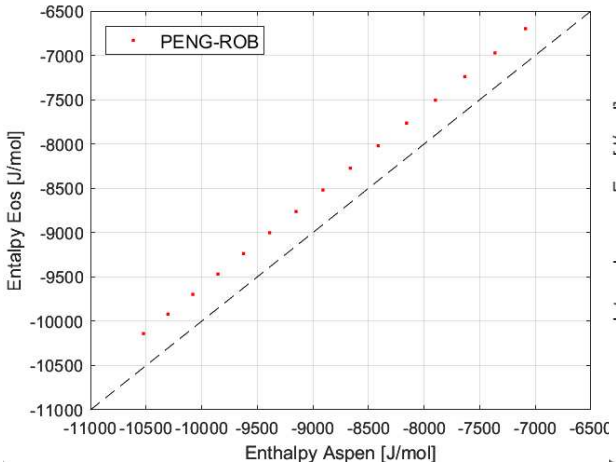

Figure 2.3: *parity plot of enthalpy.*

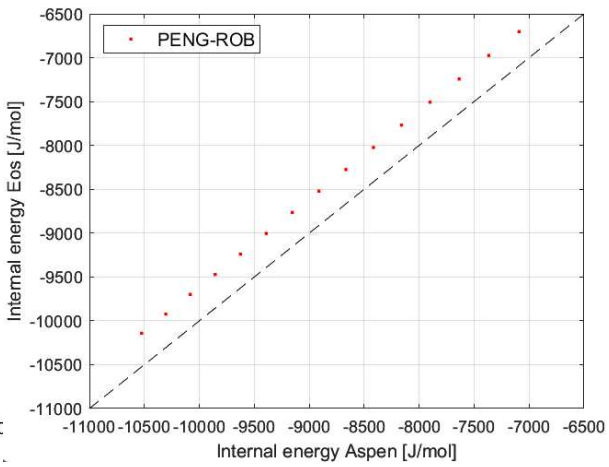

Figure 2.4: *parity plot of internal energy.*

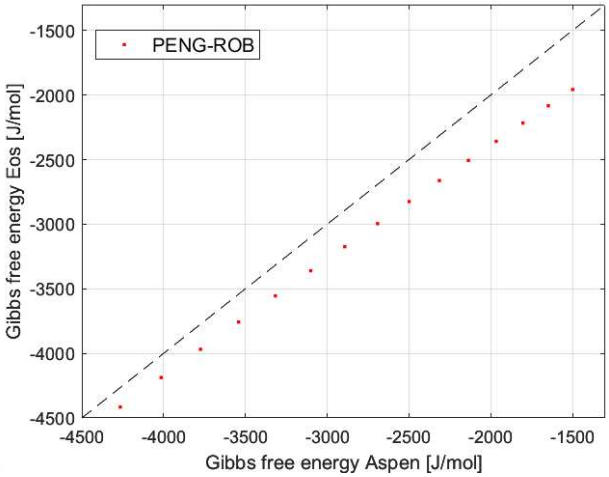

Figure 2.5: *parity plot of Gibbs free energy.*

In these plots, each point represents the estimation of a thermodynamic property, where the x-coordinate corresponds to the value calculated using the PR EoS in the process simulator, and

the y-coordinate represents the same property calculated using the JS EoS. The properties are computed at intervals of 5 K, and the closer the points are to the bisector, the more accurate the estimation of such variable. The relative error between the values computed by Aspen Plus® and those calculated with the EoS of Jäger and Span is defined as Equation 2.6 and presented in Table 2.2, where p is a generic thermodynamic property:

$$\varepsilon = \left| \frac{p_{Aspen} - p_{EoS}}{p_{EoS}} \right| \tag{2.6}$$

Table 2.2: *Relative errors in the computation of thermodynamic properties of pure solid CO_2 calculated with Peng-Robinson Eos and Jäger and Span EoS, considering a suitable temperature range for cryogenic processes. The evaluated properties are: isobar heat capacity (c_p), molar volume (v), enthalpy (h), Gibbs free energy (g) and internal energy (u).*

T [K]	Relative difference ε [-]				
	c_p [J/mol·K]	v [m³/kmol]	h [J/mol]	g [J/mol]	u [J/mol]
123.15	$6.29 \cdot 10^{-4}$	$6.50 \cdot 10^{-3}$	0.038	0.034	0.038
128.15	$1.30 \cdot 10^{-3}$	$5.60 \cdot 10^{-3}$	0.039	0.041	0.039
133.15	$3.10 \cdot 10^{-3}$	$4.60 \cdot 10^{-3}$	0.040	0.049	0.039
138.15	$4.70 \cdot 10^{-3}$	$3.60 \cdot 10^{-3}$	0.041	0.058	0.041
143.15	$5.80 \cdot 10^{-3}$	$2.50 \cdot 10^{-3}$	0.042	0.067	0.042
148.15	$6.50 \cdot 10^{-3}$	$1.50 \cdot 10^{-3}$	0.043	0.077	0.043
153.15	$6.60 \cdot 10^{-3}$	$7.95 \cdot 10^{-4}$	0.044	0.089	0.044
158.15	$6.20 \cdot 10^{-3}$	$4.42 \cdot 10^{-4}$	0.046	0.10	0.046
163.15	$5.10 \cdot 10^{-3}$	$4.05 \cdot 10^{-4}$	0.047	0.11	0.047
168.15	$3.50 \cdot 10^{-3}$	$6.91 \cdot 10^{-4}$	0.050	0.13	0.049
173.15	$1.30 \cdot 10^{-3}$	$1.30 \cdot 10^{-3}$	0.051	0.14	0.050
178.15	$1.40 \cdot 10^{-3}$	$2.30 \cdot 10^{-3}$	0.052	0.16	0.052
183.15	$4.50 \cdot 10^{-3}$	$3.50 \cdot 10^{-3}$	0.054	0.18	0.054
188.15	$8.10 \cdot 10^{-3}$	$5.20 \cdot 10^{-3}$	0.056	0.20	0.056
193.15	$1.19 \cdot 10^{-2}$	$7.10 \cdot 10^{-3}$	0.058	0.23	0.057

Accurate thermodynamic data for solid CO_2 are crucial for predicting and validating the carbon capture model. Moreover, reliable thermodynamic data for solid CO_2 help avoid incorrect equipment design operational issues such as blockages caused by unexpected CO_2 freezing. The obtained results highlight that:

- The Peng-Robinson EoS obtains results comparable with the Jäger and Span EoS for all the thermodynamic properties, the relative differences in all cases are higher increasing temperatures.
- The estimation of the solid c_p is very accurate in the whole range of temperatures.
- As expected, v is nearly constant over temperature and the major differences are in the order of 10^{-3}.

- Peng-Robinson EoS overestimates *g*. The differences with respect the solid CO_2 EoS are in the order of 5% for the three lower temperatures, increasing the temperature this deviation rises rapidly, but remaining in the order of 10% for the temperature range of greatest interest.
- The Peng-Robinson EoS underestimates *h* and *u*. However, the deviation with respect the solid CO_2 EoS is in the order of 5% or less.

In conclusion, PR demonstrates reasonable agreement with JS EoS in computing the thermodynamic properties of solid CO_2, exhibiting variations within an acceptable range. Therefore, the PR EoS can be effectively used to model the solid-vapor separation step in the CCC process.

2.2 Process modelling

The CCC process modeled and simulated in this study is based on the following assumptions:

- Pollutants such as SO_x, NO_x, HCl, CO and H_2S are not considered.
- 90% CO_2 recovery rate.
- Compressors have a polytropic efficiency of 92% (Jensen et al., 2015).
- Compression ratio cannot exceed 3.5.
- Minimum pinch temperature is 5°C for heat exchangers and 3°C for the two multi-streams heat exchangers.
- Distributed pressure drops are neglected.

2.2.1 Process description

The chemical composition and the flow specification of flue gas considered in inlet to the CCC process adhere to the reference case of Table 1.1, considering an interconnected operation mode of the cement kiln, and are reported in Table 2.3.

Table 2.3: *Flue gas flow rate, temperature, pressure and composition in inlet to the CCC process.*

	INLET FLUE GAS	
Property	**Unit**	**Value**
Total flow rate	kmol/h	10730
Temperature	°C	110
Pressure	atm	1
Gas composition		
CO_2	% mol	22.3
N_2	% mol	58.1
O_2	% mol	6.9
H_2O	% mol	12.0
Ar	% mol	0.7

The flowsheet of the process modeled in this work is provided in Figure 2.6. The flue gas exiting the cement plant (stream #1, Figure 2.6) at a temperature of 110 °C is pressurized to 1.09 bar through a blower to offset the pressure drops encountered before the main multi-stream heat exchanger (MHX1) (stream #2). Afterwards, the flue gas enters a dehydration section in which two molecular sieve beds, one operational and the other for regeneration of solid sorbent, remove the water from the flue gas (stream #7). The gas is subsequently cooled to -85 °C in the secondary multi-stream heat exchanger (MHX2) before entering the desublimation column, called also direct contact heat exchanger (stream #9). This cooling is achieved by exchanging heat with the CO_2-lean stream stream leaving the desublimation column (stream #25) and the lean slurry exiting the solid-liquid separator (stream #30). The temperature is maintained at -85 °C because it is the lowest temperature required before solid CO_2 formation, thereby preventing operational issues on the desublimation column walls. In the desublimation column, CO_2 is separated at -123 °C from the gas mixture in the solid phase due to heat transfer with the contact liquid, which is isopentane. The use of a direct heat exchanger in the CCC process offers significant advantages over indirect heat exchangers, such as resolving the issue of ice formation on the heat exchanger surface and thereby ensuring continuous operation (Asgharian et al., 2025). The slurry of CO_2/contact liquid (stream #27) produced enters a solid-liquid separator where the mass fraction of CO_2 is increased to 0.8, the molar fraction is 0.87, (stream #29) and the separated isopentane is recycled back to MHX1. Afterwards, the slurry is pressurized to 30.6 bar (stream #30) and heated in MHX2 where the solid CO_2 is melted and a biphasic liquid-vapor stream is obtained (stream #31) before entering in the final purification section. In the distillation column, the isopentane is recovered from the bottom, cooled in a heat exchanger with refrigerated water and recycled back to MHX1(stream #33). The CO_2 is collected in vapor phase from the top with a purity of 99.98% (stream #35) and pressurized to 80 bar with a compressor (stream #36) and then to 110 bar with a pump (stream #38) to meet the transportation requirements (Baxter et al., 2021). The first refrigerant loop (stream #10) consists of a hydrocarbon mixture with a molar composition of 65.26% methane, 17.39% ethane, 13.08% propane, and 4.27% butane. This mixture is compressed to 37 bar in a six-stage compressor (stream #11) and then expanded through a valve to 4.8 bar (stream #13), reaching -146°C. The second refrigerant loop uses pure CF_4, which is compressed to 29.4 bar in a 6-stage compression (stream #17) and cooled to -70°C (stream #18) in MHX2. The CF_4 is then split in three different streams: 40.22% is not expanded and enters directly to the MHX1 (stream #19), while 33.53% and 26.25% are expanded through a valve to 1.2 bar and 2 bar respectively, reaching a temperature of -125 °C and -117 °C (stream #21 and stream #23), before entering MHX1. The subsequent sections will provide a detailed analysis of the key process equipment, including the desublimation column, MHX1 and MHX2, and the compression loops. Additionally, the selection of the primary process materials, such as the contact liquid and refrigerant, will be thoroughly examined.

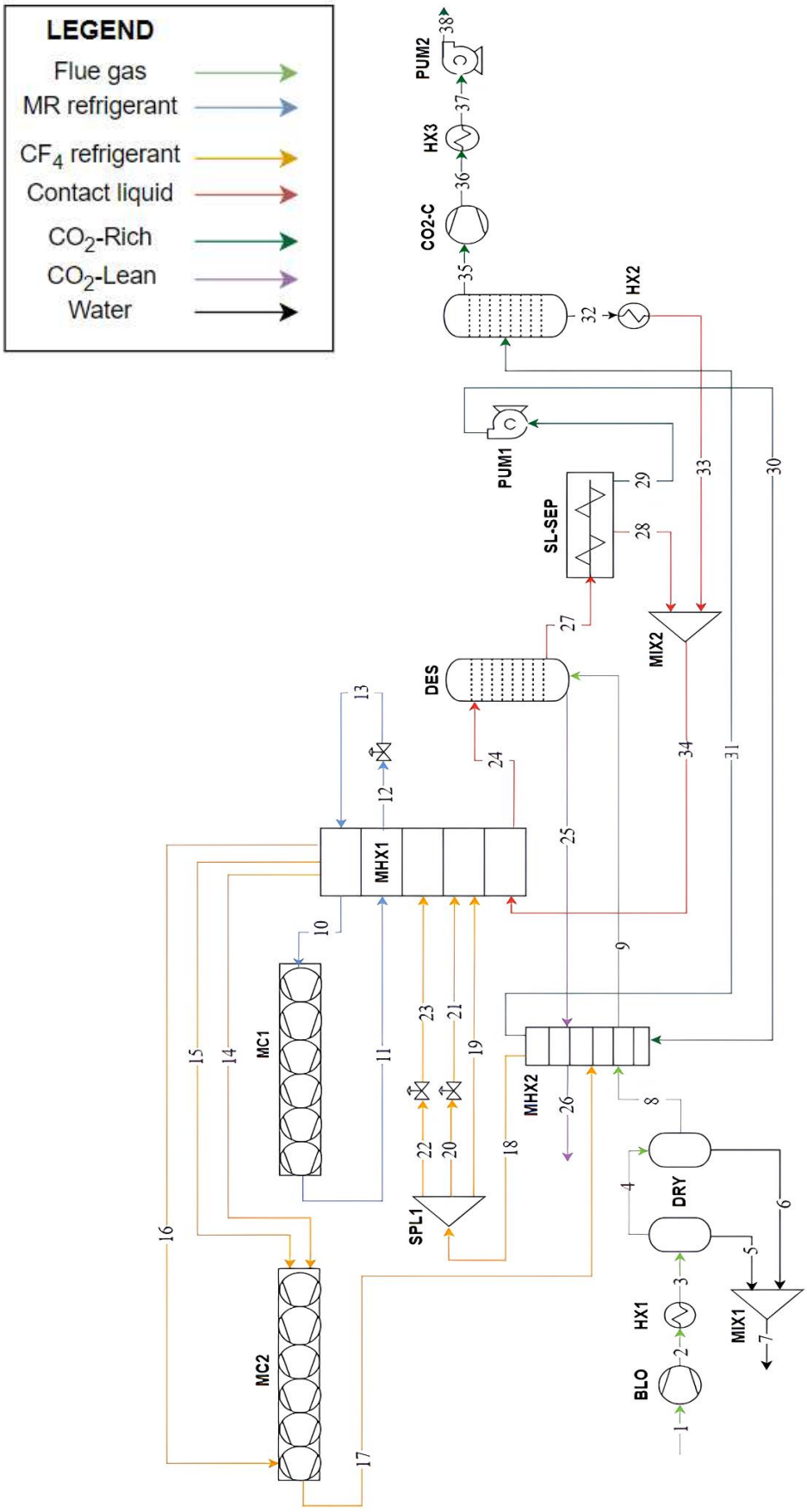

Figure 2.6: *Flowsheet of the CCC process described in Section 2.2.1.*

2.2.2 Desublimation column

The desublimation column is the key unit of the CCC process, as it facilitates the CO_2 vapor-solid phase transition through direct contact between the two phases. This equipment consists in a stainless-steel sieve trays column having from 7 to 10 stages (Figure 2.7), sieve plates create bubbles and high surface area between liquid and gas phases. As the gas cools in this column, CO_2 desublimates and entrains in the contact liquid for separation in subsequent units. The CO_2-lean gas is the vapor product from the heat exchanger column (Jensen et al., 2015).

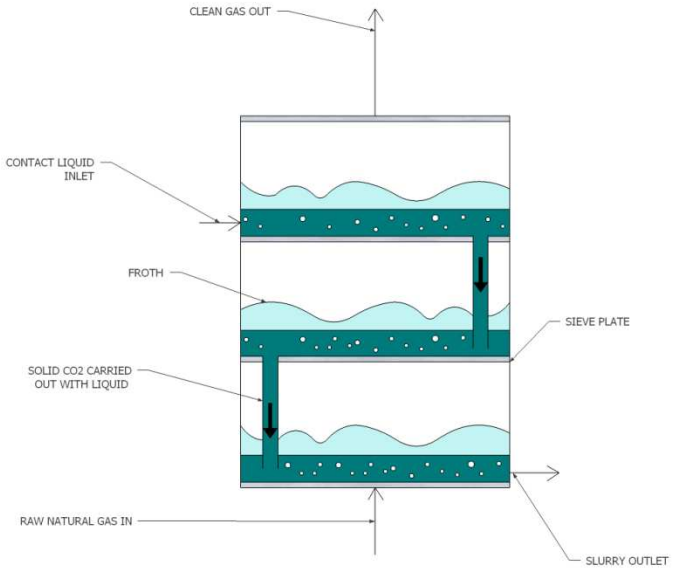

Figure 2.7: *Schematic of the desublimation column (Jensen et al., 2015).*

This type of column can be modeled with RGibbs blocks in Aspen Plus® because it is the only tool in Aspen Plus® which can calculate the phase equilibria in the presence of solids. This block determines the outlet conditions from phase equilibria calculations through a reaction-like model (Equation 2.7) by minimizing the Gibbs free energy, instead of methods based on the equality of fugacities of each component in each phase. The system is considered at equilibrium when the distribution of the components corresponds to the minimum of the Gibbs energy. (Schach et al., 2011).

$$CO_{2\,(solid)} \leftrightarrow CO_{2\,(vapor)} \tag{2.7}$$

The CO_2 capture rate, namely the amount of desublimated carbon dioxide, depends on the temperature within this operation unit. Therefore, by imposing a CO_2 recovery of 90%, it is possible to determine the flowrate of contact liquid required by the process through a sensitivity analysis of the contact liquid flowrate against the corresponding CO_2 capture rate, performed on the RGibbs block at different contact liquid temperatures (Figure 2.8).

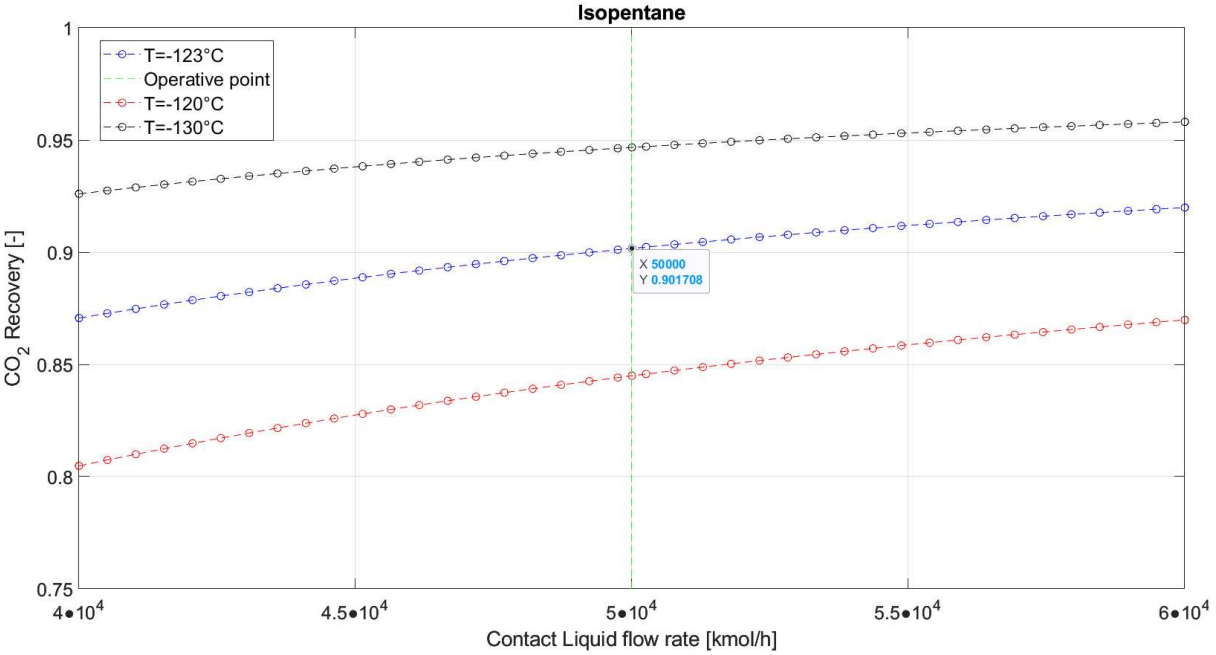

Figure 2.8: *Sensitivity analysis of contact liquid flowrate against CO_2 recovery, isopentane.*

Results show that 50000 kmol/h are needed to achieve a CO_2 capture rate of 90% and, as expected, with the same flowrate of isopentane, higher recovery values are obtained at lower temperatures. This behavior is an important because it highlights that the amount of CO_2 captured in this type of process can be easily adjusted by modifying the contact liquid temperature in the multi-stream heat exchanger, and so the energy consumption of the refrigerant loop compressors. With isopentane at -120 °C is not possible to achieve 90% of capture rate in the considered flowrate range, while contact liquid at -130 °C would require 2.24 MW of additional energy by the multi-stage compressors to obtain the same recovery and maintain a ΔT of 3°C in MHX1, even if with a contact liquid flowrate of 33000 kmol/h. Therefore, the temperature of -123 °C was chosen as a trade-off between electrical consumption and amount of isopentane required. Different contact liquids require varying flow rates to achieve comparable CO_2 recovery. This selection significantly influences the cooling demand necessary to reach the temperature corresponding to the threshold capture rate, 90%, ultimately affecting the process's overall energy consumption. In the following paragraph, three contact liquids will be compared to determine the most suitable option for the CCC process.

2.2.3 Contact liquid

The contact liquid is primarily used to prevent CO_2 solids from forming on equipment surfaces and it should be a low vapor pressure hydrocarbon, as stated in Section 1.3.2. This paragraph investigates the potential use of isobutane and propane as contact liquids, focusing on their energy requirements and related equipment dimensions. The first sensitivity analysis uses the

same approach of the one performed in Figure 2.8 to determine the required flow rate necessary to achieve the target CO_2 capture rate (Figure 2.9). The same temperatures of -120 °C, -123 °C and -130 °C are adopted in order to compare the energy consumptions of the compressors to maintain the minimum ΔT in MHX1.

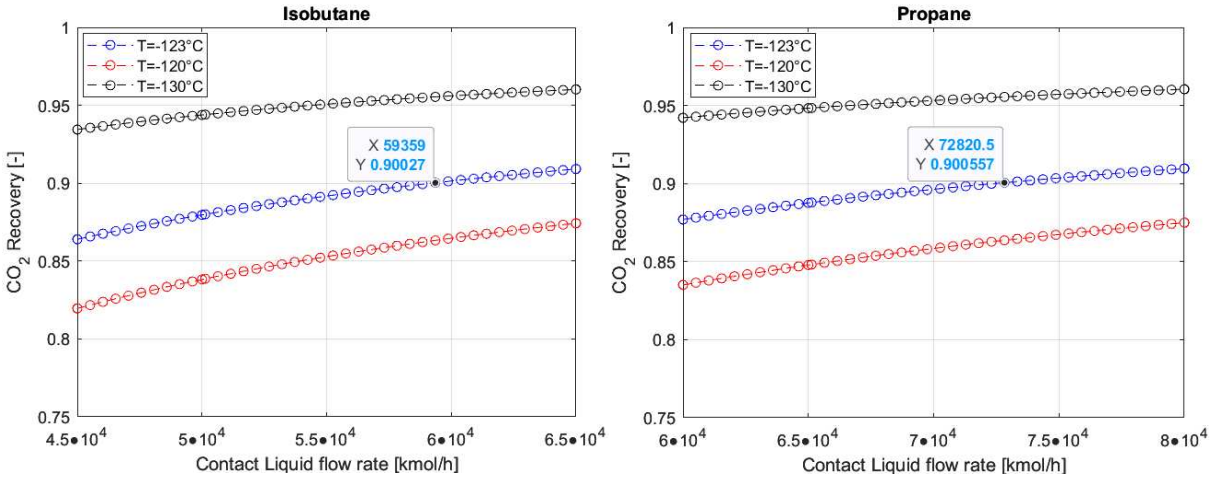

(a) *(b)*

Figure 2.9: *Sensitivity analysis of contact liquid flowrate against CO_2 recovery, isobutane (a) and propane (b).*

The flow rates required for isobutane and propane to achieve comparable CO_2 recovery are calculated as 59,400 kmol/h and 72,820 kmol/h, respectively. Both of these flow rates exceed that of isopentane, resulting in higher energy consumption for the refrigerant loops. Specifically, the use of isobutane and propane led to increased energy demands of 3.35 MW and 5.04 MW, respectively. Thus, isopentane emerges as the most energy-efficient option. The second sensitivity analysis focuses on the dimensions of the distillation column required for the CO_2-contact liquid final separation, at different operative pressures (Figure 2.10).

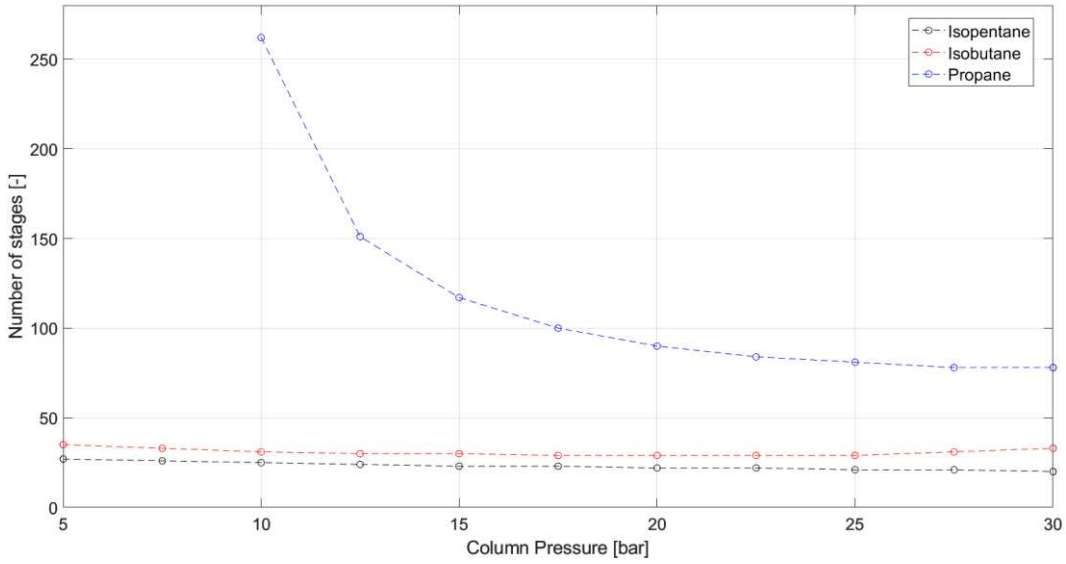

Figure 2.10: *Sensitivity analysis of distillation column operative pressure against required number of stages.*

Figure 2.10 illustrates that isopentane yields the lowest number of stages across the entire pressure range, which results in reduced equipment costs. In comparison, isobutane requires a marginally higher number of stages, between 29 and 35. Propane, on the other hand, demands a significantly greater number of stages to achieve the desired separation, underscoring its less effective performance as a contact liquid. In conclusion, the results of the sensitivity analyses identify isopentane as the most effective option for a contact liquid.

2.2.4 Multi-stream heat exchanger

The multi-stream heat exchanger (MHX) is the equipment in which the contact liquid is cooled to the desired temperature and it is the core of the process, where most of the heat exchange occurs. In Aspen Plus®, the multi-stream heat exchanger is modeled using the "MHeatX" block, which simulates heat transfer between multiple hot and cold streams. The user is required to define the inlet and corresponding outlet streams, specifying whether they are hot streams to be cooled or cold streams providing cooling energy. The outlet temperature of the hot streams is user-defined, while the outlet temperature of the cold streams is determined by the process simulator.
Multi-stream heat exchangers are Brazed Aluminum Heat Exchanger (BAHX), an example of a BAHX is provided in Figure 2.11.

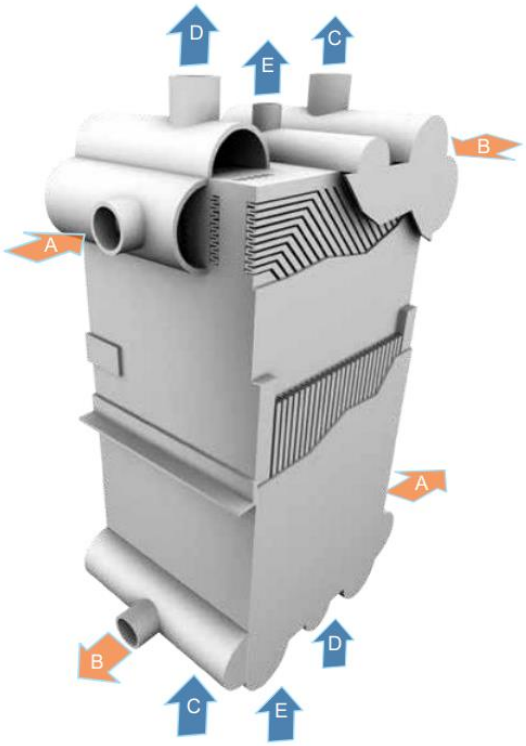

Figure 2.11: *Brazed Aluminum Heat Exchanger (Chart Industries Inc., 2023).*

Compared to a shell and tube exchanger of similar performance, a BAHX typically occupies only 20% of the space. This significant size reduction is due to its alternating plate-fin construction, which allows for multiple stream capabilities, simplifying what would otherwise require a series of shell and tube units into a single compact structure. BAHX owe their inherent versatility and high characteristics to their aluminum plate-fin construction: heat is transferred between layers across the parting sheets (primary heat transfer surface) while the fins provide an enhanced secondary heat transfer surface. Apart from the fluid entry and exit points, the edges of each layer are sealed with bars that contribute to the structure's mechanical strength and contain the fluids, preventing them from leaking to the atmosphere. This sandwich construction of layers continues in accordance with the layer stacking arrangement defined for the design until the heat exchanger block (or matrix) is complete. The multi-stream capability of the BAHX is achieved by altering the entry and exit points of each process stream, it is possible for BAHX to have 10 different process streams, or more, in a single design allowing the process designer to optimize the cooling curves for maximum process efficiency (Chart Industries Inc., 2023).

2.2.4.1 Zone analysis

The zone analysis of the multi-stream heat exchangers is an important tool to detect temperature crossovers in the system. This is represented by the intersection of the hot and cold composite curve, that characterize an unfeasible physical situation (i.e., the temperature of the cold streams is higher than the one of the hot streams). Aspen Plus® provides the zone analysis in terms of temperature against cumulative heat plots (T-q plots), dividing the axial profile of the heat exchanger in a pre-determined number of zones, and merging the hot and cold streams into one single composite curve. In this work, MHX1 and MHX2 were divided into 15 and 8 zones, respectively. Despite BAHX units are designed to operate with a minimum temperature approach of 1 °C (Chart Industries Inc., 2023), in this thesis a minimum ΔT of 3 °C is assumed to have a more flexible operation and avoid any risk of temperature crossover. Increasing the minimum ΔT along the MHX profile leads to higher energy consumptions by the compression systems, since the refrigerant should be maintained at lower temperatures.
The cooling energy is supplied by the refrigerant loops, and the choice of refrigerant influences the behavior of the T-q diagram. In this study, the use of CF_4 and LNG as potential refrigerants for the second cooling loop is investigated. Consequently, two separate analyses were conducted for MHX1, utilizing either CF_4 or LNG in combination with the mixed refrigerant from the main compressor loop. These analyses are presented in Figures 2.12 and 2.13, respectively, to identify the most suitable refrigerant for this process. Additionally, the minimum ΔT along the heat exchanger, known as the pinch point, is emphasized in each plot.

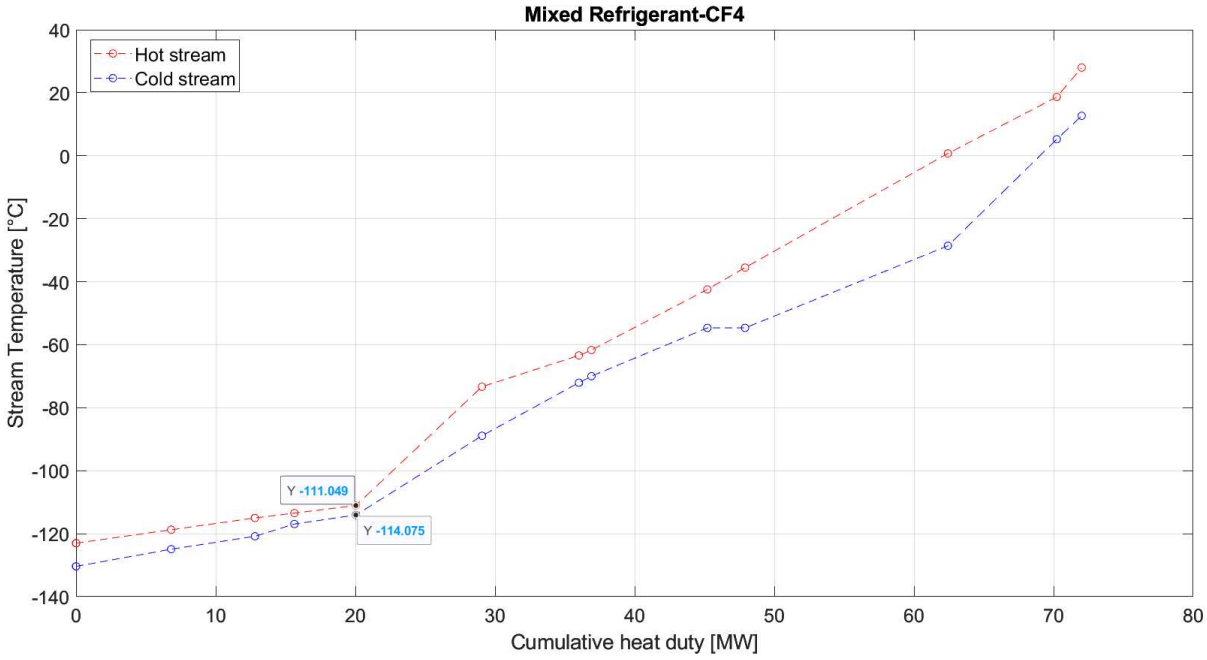

(a)

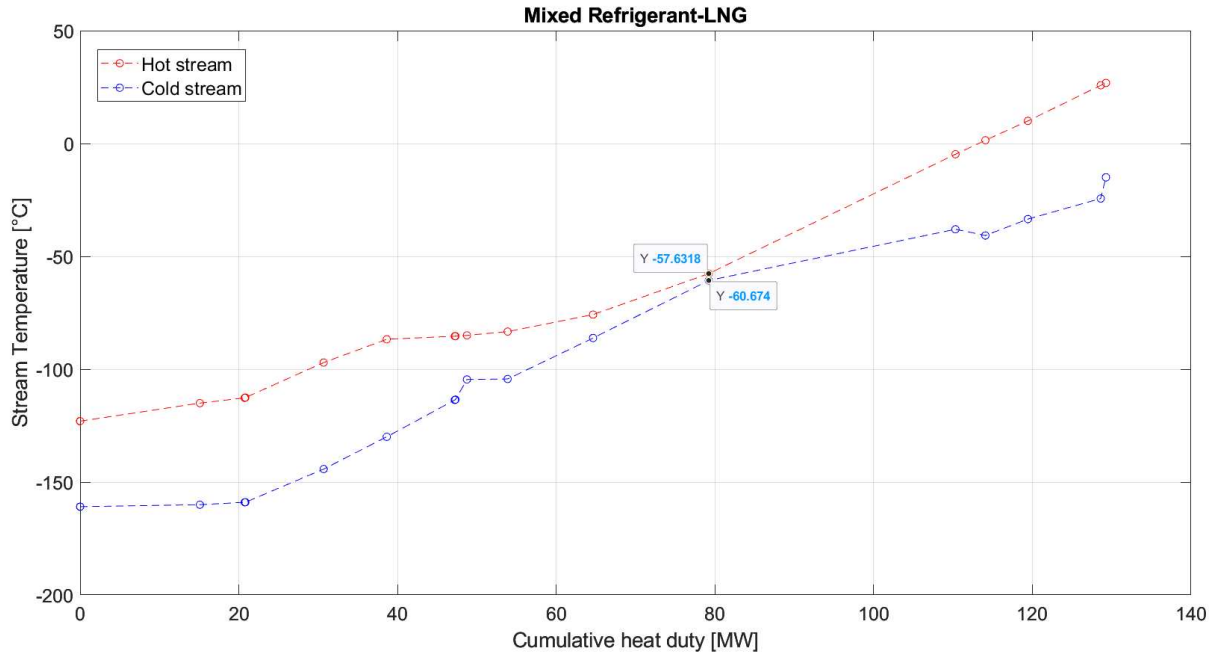

(b)

Figure 2.12: *MHX1 zone analysis with C1-C4 mixture and CF_4 as refrigerants (a) and with C1-C4 mixture and LNG as refrigerants (b). The red line represents the hot composite curve, generated by Aspen Plus®, which consolidates the hot streams to be cooled within the MHX to the target temperature. Similarly, the blue line corresponds to the cold composite curve, derived from the cold streams supplying the necessary cooling energy.*

Figure 2.12 (a) illustrates that, when CF_4 is used as the refrigerant, the cold stream curve more consistently follows the hot stream curve and remains closer to it at both extremes. In contrast,

Figure 2.12 (b) shows that the composite curves exhibit a significantly larger ΔT within the ranges of 0 MW to 60 MW and 100 MW to 130 MW. This suggests that excess cooling energy is supplied to bring the contact liquid at the desired temperature of -123 °C, leading to an increase of the overall process energy consumption. The zone analysis for MHX2, presented in Figure 2.14, confirms the absence of temperature crossovers between the process streams. Additionally, it verifies that the minimum internal temperature difference of 3°C is satisfied in this equipment.

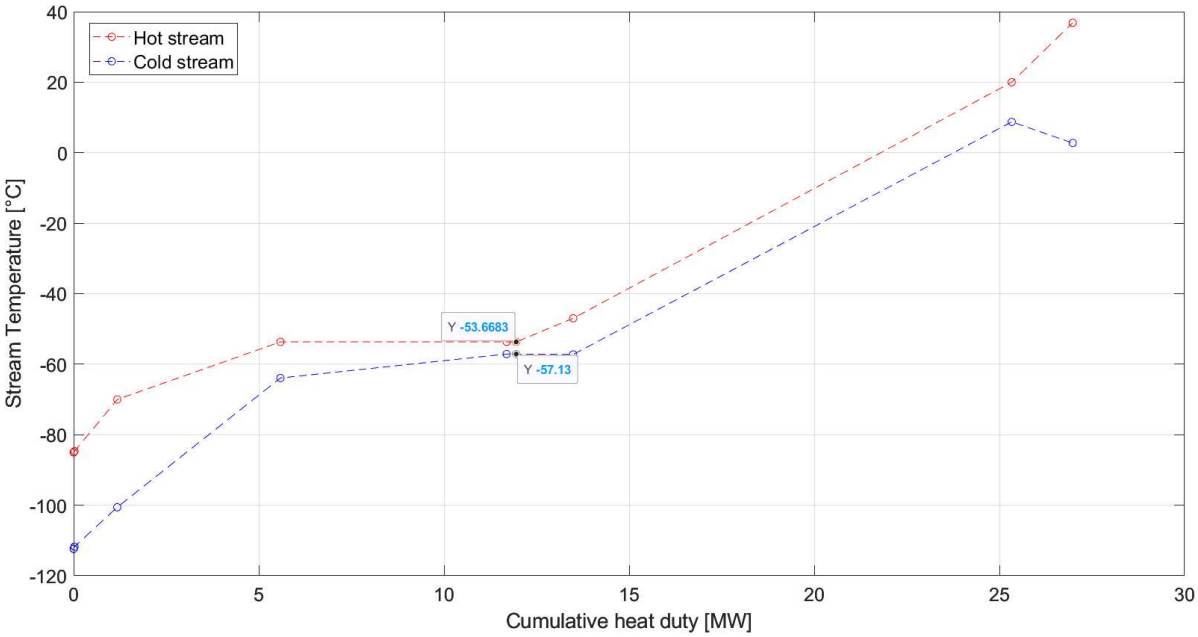

Figure 2.13: *MHX2 zone analysis between process streams.*

2.2.5 Refrigerant loops

Refrigerants acts as the cooling system to bring the recycled contact liquid back to -123 °C after being separated from the CO_2. At this stage, the temperature of the recycled contact liquid is -111°C (stream #34 in Figure 2.6). The main loop is characterized by a mixed refrigerant, namely a mixture of C_1-C_4 hydrocarbons. This type of refrigerant can provide desired refrigerant characteristics such as closely matched hot and cold composite curves and small temperature driving forces over the whole temperature range, ultimately reducing the shaft work required for compression. Also, a mixed refrigerant system features a simpler machinery configuration and fewer maintenance problems (Perry et al., 2008).

The required mixed refrigerant flowrate is 12000 kmol/h, which is compressed to 37 bar in 6 stages, after each compression stage a stainless steel plate and frame heat exchanger cool down the refrigerant to 28 °C using refrigerated water. An increase in the number of compression stages results in reduced electricity consumption but incurs higher capital costs. For this study,

a six-stage configuration was selected as a compromise between minimizing operational energy consumption and managing capital expenditure, while also ensuring the required compression ratio is achieved. Moreover, CCC processes commonly utilize refrigerant loops with 5 to 10 stages, as noted by Jensen et al. (2015). Following the compression, the refrigerant passes through MHX1 exchanging heat with the expanded refrigerant reaching a temperature of -115 °C before being expanded in a valve to 4.8 bar and being cooled to -130 °C. This loop is the most energy intensive step of the process requiring 18.00 MW. The second refrigerant loop requires 8.27 MW when using CF_4, compared to 30.80 MW when using LNG to achieve the same ΔT in the zone analysis plots (Figures 2.12a and 2.12b). This demonstrates the superiority of CF_4 as a refrigerant in terms of energy efficiency, as anticipated in Section 2.2.4.1. The required flowrate of CF_4 is 5040 kmol/h.

CF_4 refrigerant loop cools the isopentane in a more selective way by being split in 3 different streams, each one expanded to a different pressure as explained in Section 2.2.1. Splitting the refrigerant stream leads to a much lower energy consumption. Considering the T-q diagram of MHX1 (Figure 2.12a), in the zones where the ΔT between the hot and cold stream is already high we can avoid to expand all the CF_4 flowrate to very low temperatures. For example, the ΔT at the coldest extreme of MHX1 is higher than 15 °C thanks to the mixed refrigerant loop, so it is not necessary to expand all the CF_4 stream to low pressures and waste energy. Instead, it is possible to expand only a portion of refrigerant to a specified temperature that will act selectively in the specific portion of the zone analysis where ΔT is lower and there is a risk of temperature crossover.

The disadvantage of using CF_4 is its high Global Warming Potential (GWP), estimated as 6630 (Pachauri and Meyer, 2014). Then, it is of paramount importance regular maintenance and inspections of this refrigerant loop to prevent leakages in the atmosphere.

2.2.6 Purification section

The purification section comprises the solid-liquid separator, the distillation column, which separates the CO_2 from the residual contact liquid, and the final pressurization to 110 bar to meet the pressure requirements for transportation.

In the process simulator, the column is modeled with the “RadFrac” model, a 99.5% recovery of inlet CO_2 and a 99.99% of CO_2 purity in the top stream are selected as design specifications. The column input parameters to achieve +99.99% purity of CO_2 in the distillate are described as follows:

- Number of theoretical stages and feed stage: 22 and 13 respectively.
- Number of real stages and feed stage (tray efficiency of 0.6 is assumed): 37 and 22 respectively.

- Partial condenser.
- Reflux ratio: 0.28.

The distillation column was selected to operate at a pressure of 30 bar, as elevated pressures typically result in smaller equipment, leading to fewer stages (as demonstrated in Figure 2.10) and smaller column diameters. Furthermore, higher pressure leads to increased vapor and liquid densities, which promotes greater mass transfer rates, and the higher pressure is often associated with elevated temperatures, improving heat transfer in both reboilers and condensers, thereby improving energy efficiency. An increase in pressure reduces relative volatility, leading to more challenging separation, however, no significant separation or convergence issues are encountered within the distillation column. (Liu and Jobson, 1999).
The reboiler duty increases with pressure, however this difference between 5 bar and 30 bar entails an increase in the medium-pressure steam (MPS) flowrate of 0.91 kg/s (Figure 2.15), which is, considering also the associated operative costs, minor compared with the other utilities in the process.

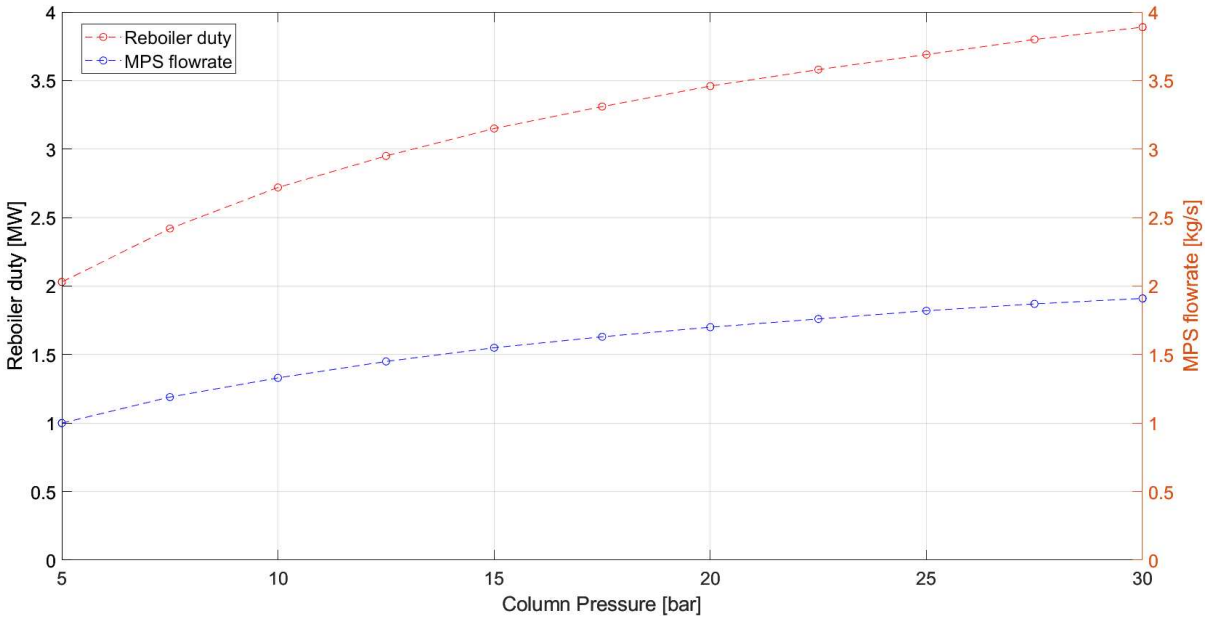

Figure 2.14: *Reboiler duty and corresponding MPS flow rate against distillation column operative pressure.*

Based on these specifications, the dimensions of the distillation column are as follows:

- Section 1 diameter (from stage 2 to stage 18): 1.52 meters.
- Section 2 diameter (from stage 19 to stage 36): 1.67 meters.
- Height: 24.74 meters.

25.84 kg/s of pure vapor CO_2 exits from the top of the column and 1.15 MW and 0.17 MW are required by the CO_2 compressor and pump respectively to pressurize this stream to 110 bar.

2.3 Economic model

This section provides the methodology developed for conducting the economic analysis of the CCC process investigated. The analysis includes the estimation of capital and operational expenses, which are then entering the calculation of economic KPIs. Firstly, the purchase costs of the equipment are determined by costing correlations. Installation costs are subsequently estimated through Bare Module Factors, adjusted with CEPCI index for January 2024 (795.4) and considering a US Dollar to Euro conversion rate of 0.91. Finally, capital and operative costs of the plant are obtained adhering to the procedure proposed by Rubin at al. (2013).

2.3.1 Equipment cost

The purchase cost, C_p^0, all the compressors, the heat exchangers, columns, and for the centrifugal pump PUM1 is calculated from Turton et al. (2018: Appendix A) through Equation 2.8.

$$\log_{10} C_p^0 = K_1 + K_2 \log_{10}(A) + K_3[\log_{10}(A)]^2 \tag{2.8}$$

Where A is the size parameter, the shaft power in kW for compressors and pumps, the surface in m^2 for heat exchangers and the volume in m^3 for towers, and K_i are tabulated constants.
The installation cost, C_{BM},is then obtained multiplying the purchase cost by the Bare Module Factor, F_{BM} (Equation 2.9).

$$C_{BM} = C_p^0 F_{BM} = C_p^0(B_1 + B_2 F_M F_P) \tag{2.9}$$

where F_M is the material factor, F_P the pressure factor and B_i are tabulated constants.
The distillation column is considered as a sum of a vertical vessel, trays and a kettle reboiler, while the intercoolers in the refrigerant loops are assumed as plate and frame heat exchangers. The material of construction of these units is stainless steel, since it avoids corrosion issues and it is suitable for cryogenic temperatures (Green and Southard, 2019). Table 2.4 and Table 2.5 present the parameters utilized in Equations 2.8 and 2.9, respectively, to calculate the associated purchase and installation equipment costs.
The cost of liquid CO_2 pump, PUM2, is calculated using the relationship proposed by Cinti et al., 2018 (Equation 2.10).

$$C_p^0\ [M€_{2011}] = 1.66\left(\frac{P_S\ [kW]}{1200}\right)^{0.85} \tag{2.10}$$

The installation cost is estimated as 2/3rd of the C_p^0 and updated with the CEPCI index.

Table 2.4: *Size parameters and constants to calculate C_p^0 of the following units (Turton et al., 2018: Appendix A).*

$\log_{10} C_p^0 = K_1 + K_2 \log_{10}(A) + K_3[\log_{10}(A)]^2$				
Equipment	K_1	K_2	K_3	A
MC1 Compressors	2.2897	1.3604	-0.1027	P_S [kW]
MC1 Intercoolers	4.8306	-0.8509	0.3187	A [m^2]
MC2 Compressors	2.2897	1.3604	-0.1027	P_S [kW]
MC2 Intercoolers	4.8306	-0.8509	0.3187	A [m^2]
BLO	2.2897	1.3604	-0.1027	P_S [kW]
HX1	4.8306	-0.8509	0.3187	A [m^2]
DES Shell	3.4974	0.4485	0.1074	V [m^3]
DES Trays	2.9949	0.4465	0.3961	A [m^2]
PUM1	3.3892	0.0536	0.1538	P_S [kW]
DIST Shell	3.4974	0.4485	0.1074	V [m^3]
DIST Trays	2.9949	0.4465	0.3961	A [m^2]
DIST Reboiler	4.4646	-0.5277	0.3955	A [m^2]
HX2	4.8306	-0.8509	0.3187	A [m^2]
CO2-C	2.2897	1.3604	-0.1027	P_S [kW]
HX3	4.8306	-0.8509	0.3187	A [m^2]

Table 2.5: *Parameters used to calculate C_{BM} of the following units (Turton et al., 2018: Appendix A).*

$C_{BM} = C_p^0 F_{BM} = C_p^0(B_1 + B_2 F_M F_P)$					
Equipment	B_1	B_2	F_M	F_P	F_{BM}
MC1 Compressors	-	-	-	-	2.8
MC1 Intercoolers	1.63	1.66	2.4	1.15	-
MC2 Compressors	-	-	-	-	2.8
MC2 Intercoolers	1.63	1.66	2.4	1.10	-
BLO	-	-	-	-	2.8
HX1	1.63	1.66	1.4	1	-
DES Shell	2.25	1.82	3.1	1	-
DES Trays	-	-	-	-	1.8
PUM1	1.89	1.35	2.2	1.51	-
DIST Shell	2.25	1.82	3.1	1	-
DIST Trays	-	-	-	-	1.8
DIST Reboiler	1.63	1.66	2.4	1.12	-
HX2	1.63	1.66	1.4	1.12	-
CO2-C	-	-	-	-	2.8
HX3	1.63	1.66	1.4	1.32	-

As anticipated in section 2.2.2, the desublimation column is a stainless-steel tower. To estimate its cost, a column without condenser and reboiler is simulated in Aspen Plus® using the RadFrac model, with the inlet and outlet flowrates from the simulation. In this way, the diameter and the height of the column are obtained, and the purchase and installation cost are calculated considering the sum of the shell (vertical vessel) and the trays using Equation 2.8 and Equation 2.9 with the relative parameters.

In the study by Asgharian et al. (2025), the solid-liquid separator purchase cost is estimated at 200000 $ for an inlet mass flowrate of flue gas of 91.86 kg/s and a CO_2 mass concentration of 18.57%, using Aspen Process Economic Analyzer. As it will be detailed in Chapter 3, this value represents less than 1% of the installation costs for the multi-stage compressors. Therefore, the cost of this equipment is estimated by scaling the equipment from Asgharian et al. (2025), using the "six-tenth" rule (Equation 2.11) based on the inlet CO_2 flowrate. In the Asgharian et al. (2025), 12.28 kg/s of CO_2 exits the desublimation column in solid form, while in this study, the simulator achieves 20.83 kg/s due to variations in flue gas inlet concentrations.

$$C_P^0 = C_{P,ref}^0 \left(\frac{\dot{m}_{CO2\,(S)}}{\dot{m}_{CO2\,(S),ref}} \right)^{0.6} \tag{2.11}$$

To compute the installation cost of the solid-liquid separator, this value is updated with CEPCI index (795.4, January 2024) and them multiplied by a Lang factor of 4.7, for fluid processing plants.

To estimate the molecular sieve cost, the procedure of Walas et al. (2012) is followed. The starting point was assuming a superficial gas velocity, u_g: in this case it is set equal to 52.7 ft/min. Then, the mass transfer zone, zone of active adsorption, can be estimated trough Equation 2.12:

$$MTZ = \left(\frac{u_g}{35} \right)^{0.3} \times 1.7 \tag{2.12}$$

The height of packing bed can be calculated with Equation 2.13:

$$L = 5MTZ \tag{2.13}$$

The height of MTZ and packing bed are then calculated as 1.92 ft (0.59 m) and 9.61 ft (2.93 m), respectively. Finally, the purchase cost of the adsorption unit can be retrieved from Loh et al. (2002) as function of the packed bed length. The installation cost is estimated considering two vertical vessels in stainless-steel through Equation 2.8 and Equation 2.9, one for operation and the other to regenerate the adsorbent material. The cost of the adsorbent material itself is neglected, as it is minimal in comparison to the equipment costs.

The procedure to estimate the MHX cost follows the approach by Hewitt and Pugh (2007) and consists into several steps:

- The hot and cold composite curves are retrieved for each zone of the MHX from the zone analysis computed by Aspen Plus®.
- The mean volumetric heat transfer coefficient of each zone containing *n* streams is estimated by Equation 2.14:

$$\frac{\dot{Q}_z}{B_z} = \sum_{i=1}^{n} \frac{\dot{Q}_i}{\beta_i} \tag{2.14}$$

where $\dot{Q}_z$ is the total heat transferred in zone z, B_z is the mean volumetric heat transfer coefficient for the zone, $\dot{Q}_i$ is the heat transferred by the ith stream in the zone and β_i is the local volumetric heat transfer coefficient for the ith stream (provided in Table 2.4).

- Calculation of $\Delta T_{m,z}$ of each zone, which is provided the process simulator.
- The volume of each zone is computed with Equation 2.15:

$$V_z = \frac{\dot{Q}_z / \Delta T_{m,z}}{B_z} \tag{2.15}$$

- The total volume of the equipment, V, is then calculated from Equation 2.16, allowing 15% again for headers:

$$V = 1.15 \sum_{i=1}^{n} V_z \tag{2.16}$$

Table 2.6: *Typical values of local volumetric coefficients (Hewitt and Pugh, 2007).*

	$\boldsymbol{\beta}$ **[kW/m^3 K]**
Fluid	
Hydrocarbons liquid	1100
Boiling and condensing	1400
Gaseous: 2 bar	80
Gaseous: 20 bar	400
Air-type (O_2, N_2, etc.)	
Liquid	1000
Boiling and condensing	1200
Gaseous: 2 bar	60
Gaseous: 20 bar	300

Having established the volume, the cost of the heat exchanger can be estimated using manufacturers data for cost per unit volume as a function of volume. With this procedure, the volume of MHX1 and MHX2 are computed as 6.65 m^3 and 5.96 m^3 respectively.

2.3.2 CAPEX estimation

Following the determination of the installed cost for each piece of equipment, the total plant cost is estimated using the methodology proposed by Rubin et al. (2013), as summarized in Table 2.5.

Table 2.7: *Calculation assumptions for each capital cost elements. The followed procedure begins once the equipment installation costs are determined.*

Capital cost element	Value
C_{BM}	Installation costs
Process contingencies	30% C_{BM}
TDC	C_{BM} + Process contingencies
Engineering service (EPC)	14% TDC
Project contingencies	20% TDC
TPC	TDC + EPC + Project contingencies
Owner's and Start-up costs	10% TPC
TOC	TPC + Owner and Start-up costs

The process contingencies accounts for the level of maturity of a particular process or component within the plant, such as a CO_2 entire capture system. It attempts to quantify the additional capital costs that will likely arise as a process matures into a full-scale commercial technology. It is assumed as 30% of C_{BM} considering that the CCC technology refers to "small pilot plant data" category (Rubin et al., 2013). The sum of process contingencies and C_{BM} gives the Total Direct Cost (TDC). Engineering, Procurement and Construction (EPC) are the indirect costs related to the engineering service, while the project contingencies refer to the additional resources, set aside in a project plan to address unforeseen events, risks, or uncertainties that may arise during the course of the project. For this study, EPC are set at 14% of TDC, while project contingencies are set at 20% of TDC corresponding to "Preliminary" design effort (Rubin et al., 2013). The sum of TDC, EPC and project contingencies give the Total Plant Cost (TPC). Owner's cost constitutes a significant portion of the overall capital cost of a plant and refers to cost items that are not included in C_{BM} or EPC, such as land and permitting. The sum of TPC owner's and start-up costs give the Total Overnight Cost (TOC) that is the final element in capital costs estimation.

2.3.3 O&M estimation

Operative costs, called also Operating and maintenance costs (O&M), are categorized into fixed and variable costs. The latter include expenses related to raw material, utilities and consumables, such as electricity and chemicals used for flue gas cleanup systems. These costs are calculated by multiplying the quantity of each item used by its respective unit cost or price. Fixed costs are generally independent of plant utilization and are dominated by labor and maintenance costs. The assumptions used for estimating the O&M follow the procedure outlined by Rubin et al. (2013) and are summarized in Table 2.6.

Table 2.8: *Calculation assumptions for each O&M cost elements. Fixed operative costs (FOM) are determined by the CAPEX results, while variable operative costs (VOM) are determined from the process simulation results.*

Operative cost element	Value
Operating labor	Equation 2.18
Total maintenance	2.5% TDC
Maintenance labor	40% total maintenance cost
Administrative and support labor	30% operating labor + maintenance labor
Maintenance materials	60% total maintenance cost
Insurance	2% TDC
FOM	Sum of quantities above
Utilities	Aspen Plus®
CO_2 transport and storage	35 €/ton_{CO2}
VOM	Utilities + transport and storage
O&M	FOM + VOM

The operating labor cost is calculated estimating the number of operators and considering a salary of 60k$/year per operator. The number of work positions per shift (N_{OL}) is estimated from Equation 2.17 (Turton et al., 2018):

$$N_{OL} = \left(6.29 + 31.7P^2 + 0.23N_{np}\right)^{0.5} \tag{2.17}$$

where N_{np} is the equipment number, without considering pumps and vessels, 23 in this study, and P is the number of processing steps involving solids. The number of operators, N'_{OL}, and the operating labor cost, C_{OL}, are then obtained considering Equation 2.18:

$$N'_{OL} = 5N_{OL} \quad ; \quad C_{OL} = 60\frac{k\$}{year} \times N'_{OL} \tag{2.18}$$

The total maintenance cost is assumed as 2.5% of TPC. FOM and VOM are respectively the fixed and variable fraction of the O&M costs, their sum gives the total operative costs of the process.

The assumptions used to calculate the utilities and CO_2 transport and storage cost are reported in Table 2.9.

Table 2.9: *Utilities and CO_2 transport and storage cost.*

Operative cost element	Value	Reference
Electricity	125 €/MWh_{el}	Eurostat (2024b)
Medium-Pressure Steam	26.90 €/MWh_{th}	Inveno Inc. (2017)
Refrigerated water	0.13 €/ton	Estimated
CO_2 transport and storage	35 €/$ton_{CO2,\ cap}$	d'Amore et al. (2021)

2.3.4 Key performance indicators

Process performance is typically assessed using KPIs which are quantifiable metrics designed to evaluate the effectiveness of the proposed engineering solutions. By analyzing these metrics, it is possible to identify areas of improvement, optimize the process, and ensure that the project meets its intended targets. The KPIs investigated in this thesis are the energy penalty [MJ_{el}/kg_{CO2}], the Equivalent CO_2 Avoided Index, AC_{eq} [-], the Cost of Avoided CO_2, CAC [€/t_{CO2}] and the Specific Primary Energy Consumption for CO_2 Avoided, SPECCA [MJ_{LHV}/kg_{CO2}]. Energy penalty is the primary parameter to quantify the energetic performance of the process since the cryogenic carbon capture technology is almost completely electrified. It is defined as Equation 2.19.

$$\gamma = \frac{\dot{E}_{CCC}}{\dot{m}_{CO2}} \tag{2.19}$$

$\dot{E}_{CCC}$ represents the net power consumed by compressors, pumps and blower and $\dot{m}_{CO2}$ denotes the mass flowrate of captured CO_2.

AC_{eq} is a metric used to quantify the extent of CO_2 emissions avoidance, achieved through a specific capture technology compared to a baseline scenario and it is defined as Equation 2.20.

$$AC_{eq} = 1 - \frac{e_{clk,eq,CCC}}{e_{clk,eq,ref}} \tag{2.20}$$

Where $e_{clk,eq,ref}$ is the sum of the direct specific CO_2 emissions at the cement kiln stack and the indirect specific CO_2 emissions, due to the use of electricity and steam consumption, of the reference case, namely the clinker production process without the CCC technology. $e_{clk,eq,CCC}$ refers to the same quantity considering the CO_2 capture process associated to the cement plant (Anantharaman et al., 2017). CAC index evaluates the economic viability of carbon capture technologies, helping to guide decisions towards the most cost- effective solutions for reducing greenhouse gas emissions. It represents the additional cost to avoid emitting one ton of CO_2 through a given technology or process. The CAC is defined on Equation 2.21:

$$CAC = \frac{(COC)_{ref,CCC} - (COC)_{ref}}{e_{clk,eq,ref} - e_{clk,eq,CCC}} \tag{2.21}$$

In the numerator, the difference between the cost of clinker (COC, €/t_{clk}) of the plant with the capture process $(COC)_{ref,CCC}$ and of the reference plant without the capture process $(COC)_{ref}$ is calculated. This difference reflects the additional COC resulting from the application of the CCC process, which is an end-of-pipe technology, leaving the reference plant unchanged. Equation 2.21 can be adjusted by recognizing that the COC remains the same in both the reference cement plant and the cement plant with the carbon capture system. Therefore, the difference lies solely in the COC of the CCC process, denoted as $(COC)_{CCC}$. A similar rationale

applies to the denominator of Equation 2.21, where only the CO_2 equivalent emissions from the CCC process, $e_{eq,CCC}$, are considered. Thus, Equation 2.21 can be rewritten as Equation 2.22.

$$CAC = \frac{(COC)_{CCC}}{e_{eq,CCC}} \tag{2.22}$$

The additional COC can be estimated using Equation 2.23:

$$COC = TAC + O\&M \tag{2.23}$$

TAC is the Total Annualized CAPEX of the CCC process, considering an interest rate, i, is defined as Equation 2.24:

$$TAC = TOC\frac{i(1+i)^n}{(1+i)^n - 1} \tag{2.24}$$

SPECCA is an energy efficiency metric to measures the additional energy required to avoid the emission of a unit of CO_2, thereby assessing the trade-off between reducing greenhouse gas emissions and maintaining energy efficiency. A lower SPECCA indicates that carbon capture efforts are not leading to excessive energy use, which could diminish the environmental benefits of reducing CO_2 emissions. SPECCA is calculated using Equation 2.25:

$$SPECCA = \frac{q_{clk,eq,CCC} - q_{clk,eq,ref}}{e_{clk,eq,ref} - e_{clk,eq,CCC}} \tag{2.25}$$

In this equation, $q_{clk,eq,ref}$ represent the equivalent primary energy consumption of the reference cement plant, which is the sum of direct specific primary energy consumptions and the indirect specific energy consumptions due to the use of electricity and steam. $q_{clk,eq,CCC}$ gives the equivalent primary energy consumption of the of the cement plant with the CCC process. Thus, the numerator of Equation 2.25 indicates the additional energy required by the CCC process. Similar to the approach used for CAC, the formulation can be adjusted by considering the equivalent primary energy consumption of the CCC process, denoted as $q_{eq,CCC}$, and the equivalent emissions associated exclusively with the CCC process in the numerator and denominator, respectively. This allows the SPECCA formulation to be re-expressed as shown in Equation 2.26:

$$SPECCA = \frac{q_{eq,CCC}}{e_{eq,CCC}} \tag{2.26}$$

The reference plant data, along with the assumptions regarding indirect emissions from electricity and steam usage, are essential for calculating the KPI values. These details are comprehensively presented in Table 2.10.

Table 2.10: *Assumptions of reference cement plant production and emissions data.*

Reference Plant Data	**Units**	**Value**
Clinker production	t_{clk}/h	126
Energy assumptions		
Carbon intensity of electricity	kg_{CO2}/MWh_{el}	262
Steam emission factor	kg_{CO2}/MWh_{th}	275
Electricity generation efficiency	%	45.9

Establishing these baseline values provides a clear framework for assessing the impact of CCC technology on overall plant performance and emissions reduction. The data in Table 2.10 are retrieved by Voldsund et al. (2019).

Chapter 3

Results

In this chapter, the simulation results are presented and analyzed. The primary focus is on assessing the technical and economic performance of the CCC process, with particular emphasis on energy consumption. The chapter details the simulation findings of the CCC process, emphasizing the associated energy penalty. It provides an analysis of how key base case assumptions, such as the CO_2 capture rate, the minimum internal ΔT in MHXs, and the CO_2 inlet concentration, impact this energy penalty. Subsequently, the economic analysis section evaluates the financial feasibility of the process under study, focusing on a detailed assessment of capital and operating costs. Technical and economic results are successively used to calculate the KPIs associated with the CCC process. By comparing these indicators with commercial CO_2 capture technologies, it is possible to assess the process cost and performance effectiveness and its potential for commercial viability.
The chapter concludes with a critical discussion of the findings, identifying both the advantages and limitations of the CCC process.

3.1 Technical results

This section presents the material and energy balance outcomes from the baseline simulations conducted in this study, including the concentrations of key compounds across the different sections of the CCC process.
Subsequently, a quantitative analysis of the process behavior under varying operative conditions is provided through sensitivity analyses on the energy penalty associated with the process. This analysis offers insights into the strengths and potential limitations of the CCC process in comparison to conventional carbon capture technologies, such as amine absorption, physical adsorption, membrane processes and calcium-looping contributing to a comprehensive understanding of its effectiveness and establishing a foundation for further discussion and optimization.

3.1.1 Material and energy balance

The material balance section focuses on the quantification of all inputs and outputs within the system, ensuring that mass is conserved throughout the process. This is followed by the energy

balance, where the energy flows are reported, considering both the enthalpic changes and any work interactions within the system. The results from these balances provide critical insights into the efficiency and sustainability of the process, laying the groundwork for the subsequent simulation and performance analysis. Table 3.1 and Table 3.2 shows the full-scale Aspen Plus simulation overall mass balance and energy balance, respectively.

Table 3.1: *Overall mass balance of the CCC process simulation, with flue gas components and contact liquid as the only compounds entering or exiting the system.*

	Mass flow rates [kg/h]						
IN	**O_2**	**N_2**	**CO_2**	**H_2O**	**Isopentane**	**Ar**	**Total**
Flue gas	23691	174640	105306	23196		3000	329834
TOTAL	23691	174640	105306	23196		3000	329834
OUT							
CO_2-lean	23691	174640	12287			3000	213619
CO_2-rich			93019		15		93034
Water				23196			23196
TOTAL	23691	174640	105360	23196	15	3000	329849
IN-OUT	0.000	0.000	0.000	0.000	15.000	0.000	15.000

Table 3.2: *Overall energy balance of the CCC process simulation, considering the enthalpy flow of inlet and outlet streams and the power consumed by process equipment.*

	Sensible-Latent	**Power**	**TOTAL**
Heat In	[MW]	[MW]	[MW]
Flue gas	-340.00		-340.00
Process units		28.45	28.45
Utilities	-59.25		-59.25
TOTAL	-340.00	28.45	-370.80
Heat Out			
CO_2 poor	-30.95		-30.95
CO_2 rich	-236.28		-236.28
Water	-103.06		-103.06
TOTAL	-370.29		-370.29

In Table 3.1, "IN" denotes the stream entering the CCC process, specifically the inlet flue gas (Stream #1 in Figure 2.6). "OUT" represents the streams exiting the CCC process, which include the discharged water (Stream #7), the CO_2-lean stream (Stream #26), and the captured

CO_2 (Stream #38). The total mass balance is accurate within 0.001%, indicating no significant or hazardous material losses or accumulation in the simulation. The CO_2 collected at the outlet of the separation process achieves a purity exceeding 99.99%, which is exceptionally high. This high degree of purity enables its suitability for a range of downstream applications, including geological sequestration and the utilization of CO_2 as a chemical feedstock in various industrial processes. However, 15 kg/h of contact liquid are lost in the final product. The loss of this quantity, while not environmentally critical compared to atmospheric release, could have implications for the process performance, which are not fully understood at this stage due to the lack of full-scale implementation data. Over one operational year, assuming 8000 hours of operation, the cumulative loss of isopentane amounts to 120000 kg. Although lower contact liquid flow rates could potentially affect the CO_2 capture efficiency in the desublimation column over the long term, it is advisable to incorporate a small isopentane make-up to mitigate any adverse impacts on performance.

The CCC process energy balance is reported in Table 3.2, highlighting its electrical consumptions of the process. It achieves closure with a relative difference of 0.13%, confirming that the assumption of no heat losses from the equipment and streams.

Table 3.3 provides an overview of the species composition throughout the different stages of the process. Detailed stream tables of the whole system are reported in Appendix A.

Table 3.3: *Species molar composition through different sections of the CCC process.*

Compounds	Stream#1	Stream#8	Stream#26	Stream#27	Stream#29	Stream#35
O_2	0.069	0.078	0.101	0	0	0
N_2	0.581	0.660	0.851	0	0	0
CO_2	0.223	0.254	0.038	0.041	0.868	1
H_2O	0.120	0	0	0	0	0
Ar	0.007	0.008	0.010	0	0	0
Isopentane	0	0	0	0.959	0.132	0

The table provides an overview of the distribution of key chemical species in both the inlet stream and the outlet streams of the main process units. The data indicate that the process successfully captures CO_2 with a purity exceeding 99.99% (stream #35), while the lean-CO_2 stream exiting the process, representing the CO_2 emissions of the CCC process, (stream #26) contains less than 4% CO_2. The outlet of the desublimation column (stream #27) reveals the substantial amount of contact liquid required for the process, with the captured CO_2 representing only 4.1% of this stream on a molar basis. This concentration increases to 86.8% after the solid-liquid separation step (stream #29).

3.1.2 Energy requirements

Electrical energy consumption plays a significant role in determining the overall technical performance of the process and having also an environmental impact, due to the indirect emissions associated with the primary energy sources used for electricity generation. This section analyzes the electrical energy requirements of the CCC process in terms of energy penalty, defined as Equation 2.19. Additionally, Table 3.4 reports the electrical energy demand of each unit operation.

Table 3.4: *Breakeven of unit operation electrical energy requirements.*

Unit	Energy requirements [MW_{el}]	Electrical consumption breakeven [%]
BLO	0.76	2.67
MC1	18.00	63.24
MC2	8.27	29.06
PUM1	0.11	0.39
CO2-C	1.15	4.04
PUM2	0.17	0.60
Total	28.46	100

Multi-stage compressors in refrigerant loops are responsible for 92% of the process power consumption, with the mixed refrigerant contributing 63% and CF_4 contributing 29%. The remaining electrical energy demand is related to the blowers needed to compensate for pressure drops, and to compressors to pressurize the CO_2 outlet stream. Pumps, on the other hand, require significantly less power, making it preferable to pressurize a liquid stream instead of a gas whenever feasible.

The energy penalty calculated in the baseline simulation is 1.10 MJ_{el}/kg_{CO2}, which is lower than that of traditional carbon capture technologies discussed in Section 1.4. For instance, amine absorption incurs an energy penalty of 1.38 MJ_{el}/kg_{CO2}, in addition to requiring 3.7-4.4 MJ_{th}/kg_{CO2} of thermal energy and the use of chemical solvents (Kuramochi et al., 2012). Membrane-based technologies have an energy penalty of 1.29 MJ_{el}/kg_{CO2} (Scholes et al., 2014), while calcium-looping exhibits a lower value of 0.40 MJ_{el}/kg_{CO2}, though it also requires 2.7 MJ_{th}/kg_{CO2} of thermal energy (Vatapolous and Tzimas, 2012). The physical adsorption technique shows the lowest energy consumptions since the SARC process is completely electrified, with an energy penalty of 1.15 MJ_{el}/kg_{CO2} (Cloete et al., 2020), but remains higher than that of the CCC process. This demonstrates the superior energy efficiency of the CCC process making it a more viable option from an energetical perspective. Other studies on cryogenic solid-vapor separation exhibited even better results, i.e. lower specific electric

consumptions, for instance the studies by Asgharian et al. (2025), Jensen et al. (2015), and Baxter et al. (2021), where it ranged between 0.70 and 0.80 MJ/kg_{CO2}. The capture rate assumed in these studies is 90%, consistent with the one used in this thesis. The primary difference compared to the CCC literature is the assumption of a minimum temperature difference of 3 °C in MHX1, as opposed to the 1 °C used in those studies. This larger temperature difference requires a higher refrigerant flow rate, leading to increased electrical consumption by the compressors in the refrigeration cycles.

Figure 3.1 presents a sensitivity analysis of the energy penalty, evaluating the effects of variations in the initial assumptions made in the base case simulation. Specifically, it investigates the influence of the CO_2 capture rate and the minimum ΔT assumed in the MHXs.

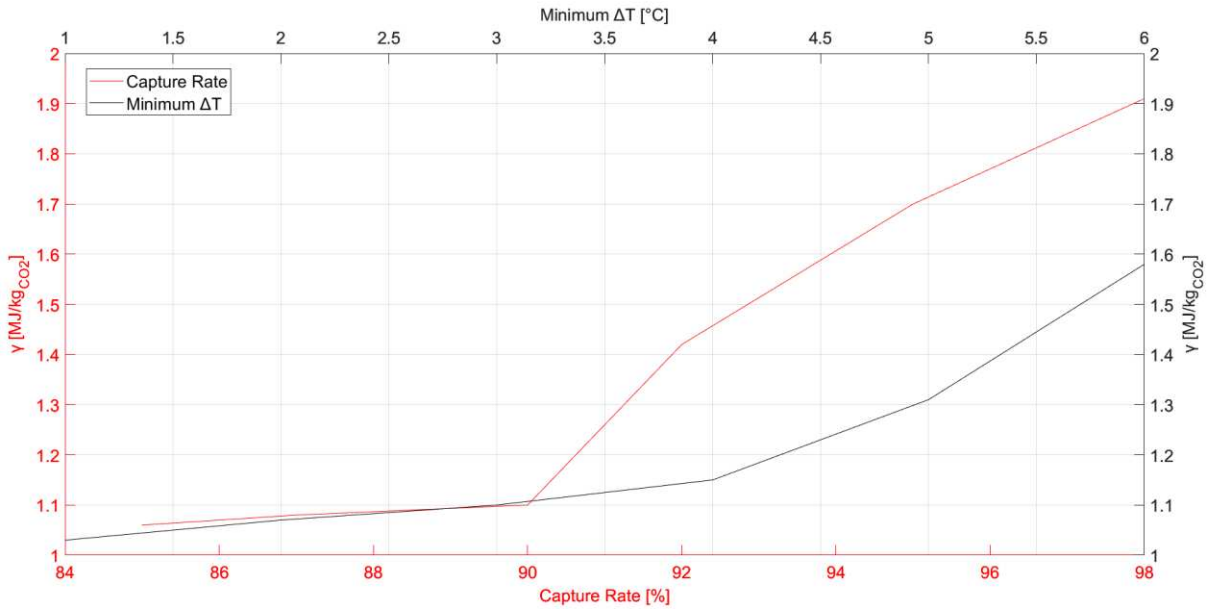

Figure 3.1: *Sensitivity analysis of energy penalty varying the base case assumptions of the CO_2 capture rate and the minimum ΔT in MHXs.*

The energy penalty from this sensitivity analysis ranges from 1.03 to 1.91 MJ_{el}/kg_{CO2}, demonstrating the competitiveness of CCC technology under varying conditions and not just in the base case. Among these two parameters, variations in the CO_2 capture rate shoes the most substantial influence on the energy penalty, exhibiting a sharp increase when the capture rate exceeds 90%. The minimum temperature difference demonstrates a similar trend; it also increases when surpassing 4 °C, although the rate of increase is less pronounced than that of the capture rate.

Nevertheless, a capture rate of 95% results in an energy penalty of 1.31 MJ_{el}/kg_{CO2}, that is comparable to, or even lower than, that of non-cryogenic techniques discussed earlier, where a 90% CO_2 capture rate is assumed. Moreover, the results underscore the robustness of the

simulated process, as no convergence issues or anomalous outcomes were observed, even when altering the initial assumptions. The results consistently lead to physically meaningful and satisfactory conclusions.

The CCC model base case achieves an energy penalty of 1.10 MJ/kg_{CO2} considering an inlet CO_2 molar concentration of 22.3%. The correlation between the energy penalty and the CO_2 inlet concentration is now investigated in Figure 3.2. A broad range of CO_2 concentrations, from 4% to 30%, was selected for analysis. A CO_2 concentration of 30% can be attained when the cement kiln operates in direct mode, where the flue gases bypass the raw mill and are routed directly to the dust filter before being emitted through the stack. This operating mode typically occurs about 10% of the time (Voldsund et al., 2019). A concentration of 18% can be observed when maintenance has not been performed for an extended period, causing the CO_2 levels to drop below the design threshold. The other concentrations investigated represent scenarios that may apply to carbon capture processes either to cement plants that are modified with particular decarbonization measures or outside of the cement sector (e.g., natural gas power plants).

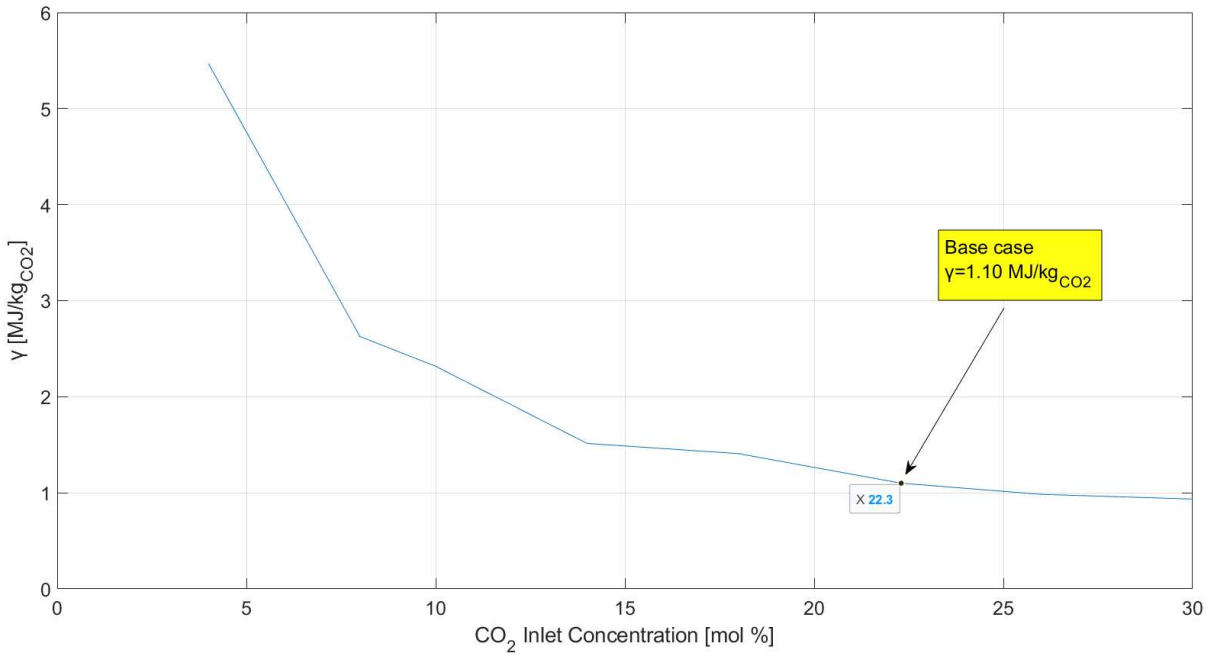

Figure 3.2: Plot of the sensitivity analysis of the *energy penalty with respect to the CO_2 inlet concentration.*

The procedure used to calculate the molar fractions of the species other than CO_2, when the CO_2 concentration changes, is known as the renormalization of molar fractions. This method preserves the relative proportions of the remaining components while ensuring that the total molar fraction equals 1. It is a standard practice in gas mixture calculations when the composition of one component is altered (Smith et al., 2018).

The energy penalty increases sharply at low CO_2 concentrations due to the reduced flowrate of captured carbon dioxide, despite energy consumption in absolute terms being comparable to

the base case of the simulation. In contrast, the energy penalty decreases at a slower rate for high CO_2 concentrations. Based on this analysis, it can be concluded that for CO_2 concentrations below 10% in the flue gas, the efficiency of CCC technology diminishes from an energy perspective, making it less advantageous than traditional methods, and therefore not recommended for such conditions. In conclusion, the energy penalty increases with a rise in the minimum internal ΔT and CO_2 capture rate. This is because the compression system requires more energy to compress and expand the refrigerant at lower temperatures compared to the base case. Additionally, the energy penalty increases as the CO_2 inlet concentration decreases. This occurs because the sublimation temperature of CO_2 decreases with lower concentrations in the mixture than the one used in the base case, thereby requiring more compression energy in such cases to achieve 90% of CO_2 capture rate.

3.2 Economic results

This section provides a detailed and comprehensive economic analysis of the CCC process. The analysis starts with a thorough evaluation of equipment costs which serve as the foundational data for determining the total plant investment required, as well as the ongoing operational expenses that will be incurred throughout the plant's lifecycle. The methodology used for these cost estimations follows the one detailed in Section 2.3. Furthermore, the results of this economic analysis are crucial for calculating KPIs related to the CCC process. These KPIs will enable the comparison of the CCC technology's economic performance with other carbon capture technologies, offering insights into its cost-effectiveness and long-term viability in industrial applications.

3.2.1 CAPEX

The installed cost of the equipment is determined using the procedure outlined in Section 2.3.1. Table 3.5 presents the individual costs of these units. Furthermore, the breakeven of these costs is discussed, highlighting the proportion of expenditures allocated to each category, thereby facilitating a more comprehensive evaluation of the economic structure of the plant.

The equipment cost estimation procedure yields results that align well with the literature. For instance, Asgharian et al. (2025) used the Aspen Plus Economic Analyzer to calculate installation costs, reporting a value of 34.40 M€, compared to 47.35 M€ in the present study. The primary discrepancy arises from the cost of the refrigerant loops; this work includes an

additional stage in the CCC process and assumes stainless steel as the construction material. Stainless steel, with its high material factor, significantly increases installation costs.

Table 3.5: *Summary of installed cost estimation, C_{BM}, for the units of the CCC process.*

Equipment	Category	C_{BM}[M€]
MC1 Compressors	Compressors, blowers, pumps	18.59
MC1 Intercoolers	Heat exchangers	4.94
MC2 Compressors	Compressors, blowers, pumps	10.88
MC2 Intercoolers	Heat exchangers	2.30
BLO	Compressors, blowers, pumps	1.17
HX1	Heat exchangers	0.34
DRY	Separators	0.68
MHX1	Heat exchangers	0.71
MHX2	Heat exchangers	0.63
DES	Columns	2.10
SL-SEP	Separators	1.45
PUM1	Compressors, blowers, pumps	0.16
DIST	Columns	0.66
HX2	Heat exchangers	0.16
CO2-C	Compressors, blowers, pumps	1.60
HX3	Heat exchangers	0.70
PUM2	Compressors, blowers, pumps	0.28
TOTAL		47.35

Compressors, blowers and pumps dominate the cost structure, accounting for 69% of the total cost. This high percentage is attributed to the significant energy demand required to compress and expand refrigerants at low temperatures, which is a core part of the CCC process. Compressors need to handle large volumes of gases, operating under high pressures to provide the necessary cooling to achieve CO_2 desublimation. Improving the efficiency of these systems could provide substantial economic benefits for the CCC process. Heat exchangers account for 21% of the total cost and, given their substantial contribution to the overall cost, optimizing the design and efficiency of heat exchangers could offer a significant opportunity for reducing operating expenses. In contrast, separators and columns together make up only 10% of the total cost. Their relatively lower expense reflects the fact that the more energy-intensive steps occur elsewhere in the process, primarily within the pressure-changing and heat exchange operations. While optimizing the design and materials of separators and columns may contribute to cost

reductions, their limited share of the total cost structure suggests that such improvements would likely have a smaller overall impact. Table 3.6 presents the CAPEX cost elements for the CCC process, following the Rubin et al. (2013) methodology outlined in Section 2.3.2.

Table 3.6: *Capital cost summary of the CCC process.*

Capital cost element	**Value [M€]**
C_{BM}	47.35
Process contingencies	14.21
TDC	61.56
Engineering service (EPC)	8.62
Project contingencies	12.31
TPC	82.49
Owner's and Start-up costs	8.25
TOC	90.74

The estimated total plant cost for the solid-vapor separation CCC process is 90.74 M€, highlighting the disadvantage of high capital investment for this technology. In comparison, membrane CO_2 capture technology for cement plants has a projected capital investment ranging from 47 M€ to 64 M€, depending on the number of membrane stages (Scholes et al., 2014). Additionally, Cloete et al. (2020) estimated a capital investment of 80 M€ for physical adsorption technology. However, the capital investment for the CCC process remains lower than that of several traditional CO_2 capture methods, such as amine absorption and calcium looping. For amine-based technologies, Antzaras et al. (2023) calculated a total plant cost of 238.26 M€ for an inlet flue gas flow rate of 14,600 kmol/h, while Nwaoha et al. (2018) estimated the capital expenditure (CAPEX) at 147 M€ for an inlet flue gas flow rate of 16,900 kmol/h. Furthermore, De Lena et al. (2019) estimated a total plant cost of 202.3 M€ for a calcium-looping CO_2 capture process. In conclusion, although the CCC process requires a substantial capital investment, it remains a viable alternative within the evolving landscape of carbon capture solutions.

3.2.2 O&M results

The operation and maintenance (O&M) costs are calculated following the methodology described in Section 2.3.3 and are summarized in Table 3.7. The fixed operating and maintenance costs (FOM) of the plant, reported in Table 2.6, are established based on the estimated CAPEX.

Table 3.7: *Operative cost summary of the CCC process.*

Operative cost element	Value [M€/year]
Operating labor	0.93
Maintenance labor	0.83
Maintenance materials	1.24
Administrative and support labor	0.53
Insurance	1.65
FOM	5.18
Utilities	31.96
Electricity	25.89
Refrigerated water	5.81
Medium-pressure steam	0.26
CO_2 transport and storage	26.05
VOM	58.01
TOTAL	63.19

In calculating the required number of work positions per shift (Equation 2.17), the number of processing steps involving solids is assumed to be zero, as the CCC process does not employ equipment such as crystallizers or crushers. However, if this number were assumed to be 1 or 2, including the desublimation column and the solid-liquid separator in this category, the corresponding number of operators would be 33 and 59, respectively. This is considered unrealistically high for a CO_2 capture system. With this assumption, the number of work positions per shift and the number of operators are estimated as 4 and 20, respectively. Variable operating costs, including utility consumption and CO_2 transport and storage, are based on process simulation results, using the price assumptions listed in Table 2.7.

The FOM costs represent only 8% of the total O&M expenses, indicating that the FOM has a minor influence on the economic results. This suggests that the economic burden of the CCC process is primarily driven by utilities consumption and CO_2 transport and storage costs (accounting for 92% of the total O&M), rather than by FOM costs associated with maintaining the facility. The limited contribution of FOM costs implies that the plant's ongoing operation is not heavily dependent on capital-intensive maintenance or infrastructure investments, but rather on the efficient management of operational units. Electricity consumption accounts for 81% of utility cost, thus the main area of improvement for the operating costs should be the refrigerant loops, MC1 and MC2.The comparison of O&M costs with literature values is challenging due to the varying assumptions regarding variable operating costs. For instance,

McKinsey (2008) estimates CO_2 transport and storage costs between 8.3 and 18.7 €/t_{CO2}, while ZEP (2011c) presents a broader range of 4.8 to 43.7 €/t_{CO2}. In contrast, IEAGHG (2017b) employs a fixed value of 10 €/t_{CO2}. In this thesis, a value of 35 €/t_{CO2} is assumed. Similarly, electricity prices reported in the literature vary significantly depending on the year of publication. Accordingly, a sensitivity of CAC varying the electricity price will be performed in the subsequent paragraphs of KPIs. Additionally, to enhance comparability with other CO_2 capture technologies, the CAC will be calculated using a representative electricity price from literature, 58.1 €/MWh_{el} (Anantharaman et al., 2017).
Figure 3.3 provides a comprehensive summary of the cost estimates detailed in Section 3.2, offering a global overview of their distribution.

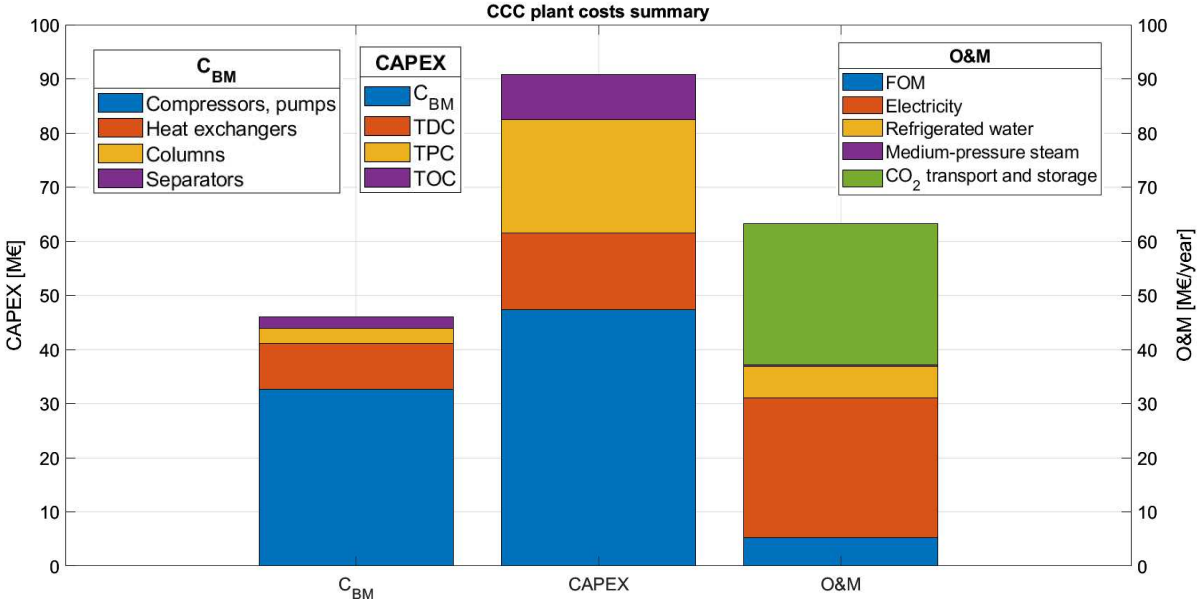

Figure 3.3: *Graphical representation of the C_{BM}, CAPEX and O&M cost elements estimated for the CCC process.*

The installed equipment costs are estimated at 47.35 M€, representing the initial cost component used to estimate the CAPEX, which amount to 90.74 M€. The CAPEX values serve as the basis for calculating FOM costs, while the VOM costs, which fluctuate in response to the system's usage and performance, are derived from simulation results. Overall, O&M costs are estimated to be 63.19 M€/year, with electricity and CO_2 transport and storage costs accounting for 82% of the total annual operating expenses.

3.2.3 Key Performance Indicators

To accurately determine the KPIs, it is essential to first establish a baseline by defining the production and energy data for the reference cement plant, without the integration of CCC technology. In this context, the analysis must also include the quantification of indirect

emissions associated with electricity consumption, as well as the thermal energy associated with steam. These data are calculated according to Table 2.10.

The first KPI evaluated is the CO_2 Avoided Index, AC_{eq}, which compares the equivalent emissions of the reference cement plant with those observed when the CCC technology is integrated. This KPI is calculated using Equation 2.20, and the equivalent emissions of the CCC process are considered as the sum of the CO_2 leaving the process in the CO_2-lean stream (direct emissions) and the emissions related to electricity and steam usage (indirect emissions).

AC_{eq} is calculated to be 81%, indicating that for every 100 units of CO_2 emissions that would have occurred in the absence of intervention, only 19 units are emitted. The integration of the CCC process results in the avoidance of 81 units of CO_2 emissions. Figure 3.4 compares the AC_{eq} index for post-combustion CO_2 capture technologies applied to the cement plant, including the one calculated in this study for the CCC process. The processes considered in the comparison include the amine absorption system, the physical adsorption (SARC), membrane processes and calcium looping (CaL). Data for this analysis were sourced from Cloete et al. (2020) for the SARC system and from Voldsund et al. (2019) for the remaining techniques.

The performance of various carbon capture technologies, as indicated by their AC_{eq} values, illustrates a competitive landscape for reducing CO_2 emissions from cement plants. Amine absorption exhibits an AC_{eq} of 64%, SARC process achieves the same value of the CCC process, 81%. The membrane process yields AC_{eq} values of 78%, while calcium looping emerges as the highest-performing technology with an AC_{eq} of 89%.

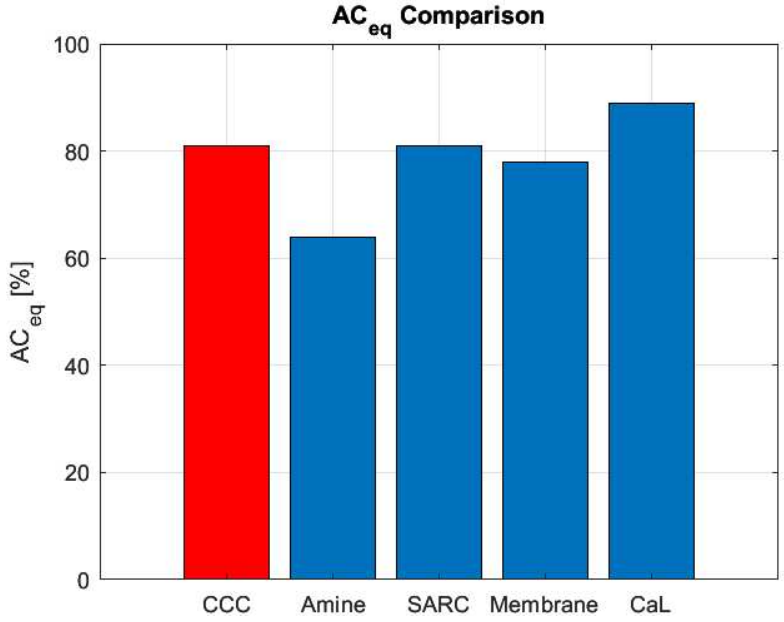

Figure 3.4: *AC_{eq} value of different CO_2 capture technologies: Cryogenic Carbon Capture (CCC), amine absorption, physical adsorption (SARC), membrane process and Calcium-looping (CaL).*

Notably, cryogenic carbon capture demonstrates a robust performance with an AC_{eq} of 81%, positioning it as a viable alternative among these technologies. Its effectiveness in reducing CO_2 emissions is comparable to the leading methods, underscoring its potential contribution to the decarbonization of cement production. SPECCA accounts for the additional energy required to prevent the emission of a unit of CO_2 and is calculated using Equation 2.26. Figure 3.5 presents a comparison of the SPECCA values for the various post-combustion CO_2 capture technologies examined in Section 1.2 of this thesis.

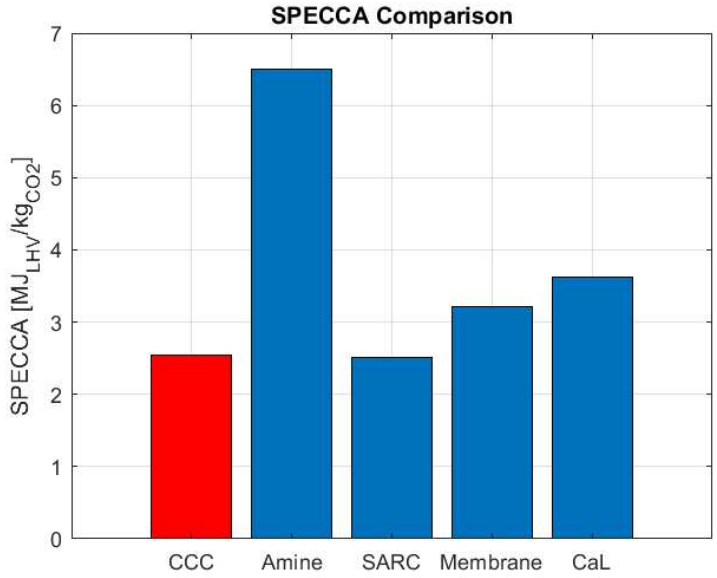

Figure 3.5: *SPECCA value of different CO_2 capture technologies: Cryogenic Carbon Capture (CCC), amine absorption, physical adsorption (SARC), membrane process and Calcium-looping (CaL).*

Cryogenic carbon capture demonstrates strong competitiveness, with a SPECCA value of 2.54 MJ_{LHV}/kg_{CO2}. This positions it favorably compared to amine absorption, which has the highest SPECCA of 6.50 MJ_{LHV}/kg_{CO2} (Jaffar et al., 2023), reflecting its poor energy performance due to the high amount of thermal energy required for solvent regeneration. Although physical adsorption (SARC process) slightly surpasses cryogenic carbon capture in energy efficiency, with a SPECCA value of 2.51 MJ_{LHV}/kg_{CO2} (Cloete et al., 2020), it achieves a lower CO_2 purity of 96%, compared to the 99.99% attained by the CCC technology. The membrane and calcium-looping processes, with a SPECCA index of 3.22 MJ_{LHV}/kg_{CO2} and 3.62 MJ_{LHV}/kg_{CO2}, respectively (Voldsund et al., 2019), are less energy efficient than the CCC process investigated. These comparisons highlight CCC as a highly competitive option, particularly when minimizing energy consumption is a critical aspect.

The final KPI analyzed is the Cost of Avoided CO_2 (CAC) as defined in Equation 2.22. The COC is determined using Equations 2.23 and 2.24, with the results for this KPI summarized in Table 3.8. Additionally, an electricity price of 58.1 €/MWh_{el}, commonly assumed in literature, is considered in the analysis. The CAC value estimated in the baseline scenario is 100.80 €/t_{CO2}.

Table 3.8: *Cost of Clinker (COC) and Cost of Avoided CO_2 at different electricity prices.*

Electricity price [€/MWh_{el}]	COC [€/t_{clk}]	CAC [€/t_{CO2}]
125	70.75	100.80
58.1	57.55	81.99

It is evident that, since operational costs dominate and the CCC process is highly dependent on electricity, variations in electricity price assumptions result in significantly different estimations of this KPI, as shown in Table 3.8. For this reason, a sensitivity of CAC varying the electricity price is performed in Figure 3.6.

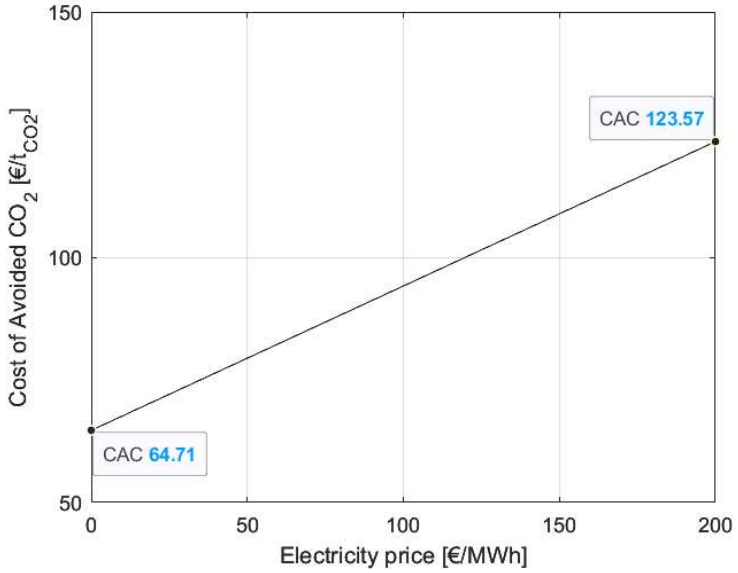

Figure 3.6: *Sensitivity analysis of the CAC varying the electricity price.*

The CAC varies between 64.71 €/t_{CO2} and 123.57 €/t_{CO2} for electricity prices ranging from 0 €/MWh_{el} to 200 €/MWh_{el}. By comparing these values with the base case, the contribution of individual cost components to the CAC can be determined: FOM costs account for 9.3% and annualized CAPEX make up 14.1%, while electricity represents 38.0% of the total CAC and CO_2 transport and storage contributes 38.6%. These two categories are the primary drivers of this KPI, accounting for nearly 77% of the total CAC. This underscores their significant influence on the overall financial sustainability of the project.

The CAC, as calculated in Table 3.8, is then compared in Figure 3.7 (a) with the capture technologies discussed in Section 1.2. Given that many studies in the literature exclude CO_2 transport and storage costs in their economic assessments of operational expenses, Figure 3.7 (b) presents the same comparison that neglects these costs within the CCC process, enabling a more consistent and robust comparison of the data.

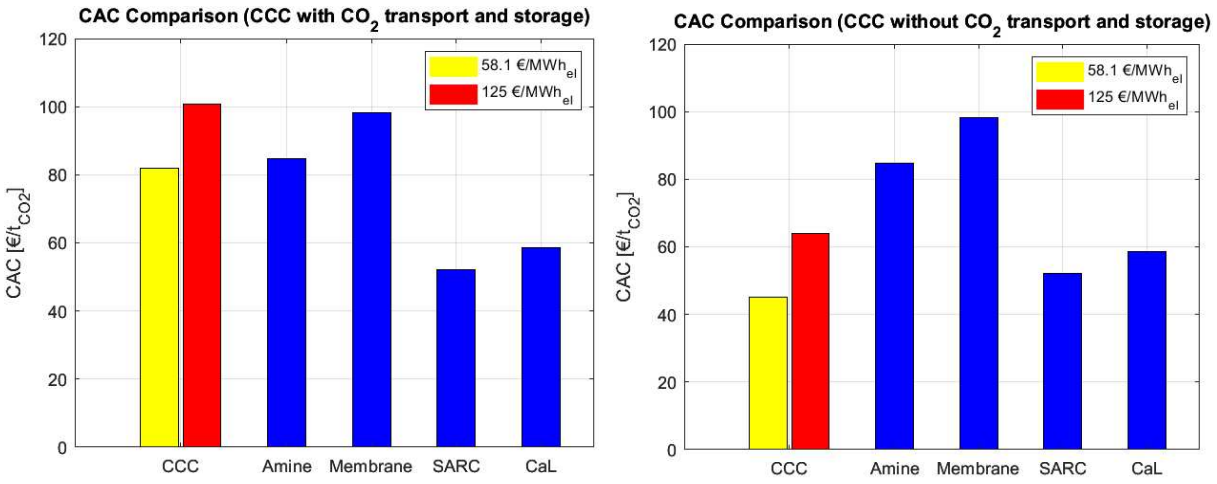

(a) *(b)*

Figure 3.7: Comparison of CAC values for various CO_2 capture technologies. In the left-hand figure (a), CO_2 transport and storage are included in the operative cost calculation for the CCC process, while in the right-hand figure (b), these costs are excluded.

In Figures 3.7 (a) and (b), the yellow bar represents an electricity price of 58.1 €/MWh_{el} and the red bar denotes the electricity price of 125 €/MWh_{el}, selected as the baseline assumption. The CAC values for various carbon capture technologies demonstrate significant performance differences, primarily influenced by electricity price assumptions and the inclusion of CO_2 transport and storage costs. When CO_2 transport and storage are included in the operational costs, the CCC process exhibits CAC values ranging from 81.99 €/t_{CO2} to 100.80 €/t_{CO2}, depending on the electricity price. By comparison, amine absorption, evaluated for an electricity price of 115 €/MWh_{el}, shows a CAC of 84.70 €/t_{CO2} (Jaffar et al., 2023). For physical adsorption, membrane processes, and calcium-looping, with an electricity price of 58.1 €/MWh_{el}, the CAC values are 52 €/t_{CO2} (Cloete et al., 2020), 98.17 €/t_{CO2} (Scholes et al., 2014), and 58.6 €/t_{CO2} (De Lena et al., 2019), respectively. It is important to note that for these technologies, CO_2 transport and storage costs are not included in the operative costs estimation. When CO_2 transport and storage are similarly excluded from the CCC process, the CAC decreases to 45.23 €/t_{CO2} and 63.98 €/t_{CO2}, across the abovementioned electricity price assumptions. This significant reduction highlights the cost-competitiveness of the CCC process when evaluated under the same assumptions as the other technologies. Under these comparable conditions, CCC outperforms alternative carbon capture technologies. For example, at an electricity price of 58.1 €/MWh_{el}, CCC achieves a CAC which is not only lower than the calcium-looping process (58.6 €/t_{CO2}) but also competitive with physical adsorption (52 €/t_{CO2}). These results underscore the potential of CCC as an economically favorable option for CO_2 capture. CCC emerges as an attractive alternative for cement plant CO_2 mitigation. Therefore, the CCC process could play a critical role in decarbonizing cement plants and industries that

rely heavily on electricity, offering a cost-effective and scalable solution for reducing carbon emissions compared to other available technologies.

Conclusions

In this study, a thorough techno-economic analysis of the Cryogenic Carbon Capture (CCC) process was conducted to assess its potential in capturing CO_2 emissions from cement plant flue gases. The primary aim was to evaluate the effectiveness of CCC technology as a sustainable alternative to traditional carbon capture methods, with the goal of promoting its broader industrial use.

The CCC process was simulated in Aspen Plus® to evaluate its capability of producing a purified CO_2 stream from a flue gas flow rate of 10730 kmol/h, meeting the standards for transportation and storage. Before the simulation, a validation process compared the thermodynamic properties of solid CO_2 from the Peng-Robinson EoS in Aspen Plus® with those from the Jäger and Span EoS. The results showed a 6-10% relative error in Gibbs free energy estimates within the temperature range from -130 °C to -115 °C, particularly affecting the desublimation column, which uses a Gibbs reactor model. Therefore, experimental validation is suggested to improve predictions regarding the vapor-solid CO_2 phase transition.

The simulation results indicate that the CCC process can achieve a 90% CO_2 recovery rate with a purity greater than 99.99%, which enhances both compliance with regulatory standards and the commercial value of captured CO_2. This high-purity CO_2 opens possibilities for monetizing emissions, improving the economic feasibility of CCC. However, a loss of 15 kg/h of contact liquid in the final CO_2 stream was observed. To sustain long-term capture efficiency, periodic isopentane make-up is recommended. The process relies almost on electricity, with the compressors in the refrigerant loops driving the system's energy requirements. The energy penalty for the CCC process is 1.10 MJ_{el}/kg_{CO2}, lower than that of many conventional carbon capture technologies such as amine absorption, physical adsorption, membrane processes, and calcium looping. Even under varying operational parameters, the energy penalty does not exceed 1.91 MJ_{el}/kg_{CO2} for a CO_2 recovery of 98%, demonstrating CCC's competitiveness and adaptability in different conditions. However, the energy penalty increases when CO_2 inlet concentrations fall below 10%, as additional energy is required to sustain desublimation conditions in more diluted flue gas mixtures. As a consequence, from an energy perspective, the CCC process becomes less advantageous when compared to established carbon capture technologies.

Economically, the capital expenditure (CAPEX) for the CCC plant is estimated at 90.74 M€, with installation costs of 47.35 M€ driven primarily by the two compression systems. The operational costs are projected at 63.19 M€, heavily influenced by electricity costs (125 €/MWh_{el}), as well as CO_2 transport and storage expenses. These assumptions complicate comparisons with existing literature due to differences in assumptions, such as publication year. Key performance indicators (KPIs) analyzed include the CO_2 Avoided Index (AC_{eq}), Specific

Primary Energy Consumption for CO_2 Avoided (SPECCA), and the Cost of Avoided CO_2 (CAC).

The SPECCA value of 2.54 MJ_{LHV}/kg_{CO2}, comparable to physical adsorption technologies, further highlights its energy-efficient capture performance, making it highly suitable for energy-intensive industries. Although the CCC process appears cost-intensive with a CAC of 100.80 €/t_{CO2}, when normalized under consistent assumptions, its CAC drops to 45.23 €/t_{CO2}, establishing CCC as economically competitive compared to traditional methods. Moreover, the potential to retrofit CCC technology into existing infrastructure reduces capital costs, enhancing its appeal for large-scale deployments.

The conclusions of this study underscore CCC as a technologically advanced and economically viable CO_2 capture solution, especially for high-emission industries like cement production. Its strengths lie in high CO_2 purity, energy efficiency, and cost-effectiveness. However, further validation is required for some assumptions. Notably, experimental validation is needed to address practical issues not captured in the theoretical model, such as heat losses and distributed pressure drops, which could elevate the process' energy demands. The potential environmental impacts from the water content removed during drying, which may contain dissolved impurities, also require investigation to ensure compliance with emission standards. Furthermore, plant costs are estimated based on literature correlations, which may result in deviations from actual market prices. For a more accurate assessment, it is advisable to gather real cost data from existing plants and consult equipment manufacturers to obtain reliable estimates for both equipment and overall plant expenses.

In conclusion, CCC emerges as a promising technology capable of significantly reducing greenhouse gas emissions, offering a sustainable path forward to cement industry.

Appendix A

Stream table

Stream # in Fig. 2.6	**1**	**2**	**3**	**4**	**5**	**6**	**7**
Mole fractions [-]							
CO_2 (S)	0	0	0	0	0	0	0
CO_2	0.223	0.223	0.223	0.249	0	0	0
O_2	0.069	0.069	0.069	0.077	0	0	0
N_2	0.581	0.581	0.581	0.646	0	0	0
H_2O	0.120	0.120	0.120	0.020	1	1	1
Ar	0.007	0.007	0.007	0.008	0	0	0
CH_4	0	0	0	0	0	0	0
C_2H_6	0	0	0	0	0	0	0
C_3H_8	0	0	0	0	0	0	0
n-C_4H_{10}	0	0	0	0	0	0	0
i-C_5H_{12}	0	0	0	0	0	0	0
CF_4	0	0	0	0	0	0	0
Total Flow [kg/h]	329834	329834	329834	309898	19936	3260	23197
Total Flow [kmol/h]	10730	10730	10730	9623	1107	181.0	1287
Molar vapor fraction [-]	1	1	0.912	1	0	0	0
Molar liquid fraction [-]	0	0	0.088	0	1	1	1
Molar solid fraction [-]	0	0	0	0	0	0	0
Temperature [°C]	110	118	30	30	30	30	30
Pressure [bar]	1.01	1.09	1.09	1.09	1.09	1.09	1.09
Density [kg/m^3]	0.98	1.03	1.36	1.34	999	999	999

Stream # in Fig. 2.6	**8**	**9**	**10**	**11**	**12**	**13**	**14**
Mole fractions [-]							
CO_2 (S)	0	0	0	0	0	0	0
CO_2	0.253	0.253	0	0	0	0	0
O_2	0.078	0.078	0	0	0	0	0
N_2	0.661	0.661	0	0	0	0	0
H_2O	0	0	0	0	0	0	0
Ar	0.008	0.008	0	0	0	0	0
CH_4	0	0	0.652	0.652	0.652	0.652	0
C_2H_6	0	0	0.174	0.174	0.174	0.174	0
C_3H_8	0	0	0.131	0.131	0.131	0.131	0
n-C_4H_{10}	0	0	0.043	0.043	0.043	0.043	0
i-C_5H_{12}	0	0	0	0	0	0	0
CF_4	0	0	0	0	0	0	1
Total Flow [kg/h]	306637	306637	287360	287360	287360	287360	116430
Total Flow [kmol/h]	9442	9442	12000	12000	12000	12000	1323
Molar vapor fraction [-]	1	1	1	1	0	0.101	1
Molar liquid fraction [-]	0	0	0	0	1	0.899	0
Molar solid fraction [-]	0	0	0	0	0	0	0
Temperature [°C]	30	-85	13	28	-115	-130	13
Pressure [bar]	1.09	1.01	4.8	36.63	35.89	4.8	1.96
Density [kg/m^3]	1.35	2.12	4.97	42.84	487	63.12	7.32

Stream # in Fig. 2.6	**15**	**16**	**17**	**18**	**19**	**20**	**21**
Mole fractions [-]							
CO_2 (S)	0	0	0	0	0	0	0
CO_2	0	0	0	0	0	0	0
O_2	0	0	0	0	0	0	0
N_2	0	0	0	0	0	0	0
H_2O	0	0	0	0	0	0	0
Ar	0	0	0	0	0	0	0
CH_4	0	0	0	0	0	0	0
C_2H_6	0	0	0	0	0	0	0
C_3H_8	0	0	0	0	0	0	0
n-C_4H_{10}	0	0	0	0	0	0	0
i-C_5H_{12}	0	0	0	0	0	0	0
CF_4	1	1	1	1	1	1	1
Total Flow [kg/h]	148745	178368	443543	443543	178368	148745	148745
Total Flow [kmol/h]	1690	2027	5040	5040	2027	1690	1690
Molar vapor fraction [-]	1	1	1	0	0	0	0.224
Molar liquid fraction [-]	0	0	0	1	1	1	0.776
Molar solid fraction [-]	0	0	0	0	0	0	0
Temperature [°C]	13	13	28	-70	-70	-70	-125
Pressure [bar]	1.18	28.5	29.08	28.49	28.49	28.49	1.2
Density [kg/m^3]	4.38	122	115	1213	1213	1213	39.12

Stream # in Fig. 2.6	**22**	**23**	**24**	**25**	**26**	**27**	**28**
Mole fractions [-]							
CO_2 (S)	0	0	0	0	0	0.041	0
CO_2	0	0	0.001	0.038	0.038	0	0
O_2	0	0	0	0.101	0.101	0	0
N_2	0	0	0	0.851	0.851	0	0
H_2O	0	0	0	0	0	0	0
Ar	0	0	0	0.010	0.010	0	0
CH_4	0	0	0	0	0	0	0
C_2H_6	0	0	0	0	0	0	0
C_3H_8	0	0	0	0	0	0	0
n-C_4H_{10}	0	0	0	0	0	0	0
i-C_5H_{12}	0	0	0.999	0	0	0.959	1
CF_4	1	1	0	0	0	0	0
Total Flow [kg/h]	116430	116430	3607997	213619	213619	3701016	3583856
Total Flow [kmol/h]	1323	1323	50013	7329	7329	52127	49672
Molar vapor fraction [-]	0	0.224	0	1	1	0	0
Molar liquid fraction [-]	1	0.776	1	0	0	0.959	1
Molar solid fraction [-]	0	0	0	0	0	0.041	0
Temperature [°C]	-70	-117	-123	-112	18	-112	-112
Pressure [bar]	28.49	2	1.01	1.01	1.01	1.01	1.01
Density [kg/m^3]	1213	62.29	751	2.19	1.20	753	743

Stream # in Fig. 2.6	**29**	**30**	**31**	**32**	**33**	**34**	**35**
Mole fractions [-]							
CO_2 (S)	0.864	0.864	0	0	0	0	0
CO_2	0.004	0.004	0.868	0.047	0.047	0.001	1
O_2	0	0	0	0	0	0	0
N_2	0	0	0	0	0	0	0
H_2O	0	0	0	0	0	0	0
Ar	0	0	0	0	0	0	0
CH_4	0	0	0	0	0	0	0
C_2H_6	0	0	0	0	0	0	0
C_3H_8	0	0	0	0	0	0	0
n-C_4H_{10}	0	0	0	0	0	0	0
i-C_5H_{12}	0.132	0.132	0.132	0.953	0.953	0.999	0
CF_4	0	0		0	0	0	0
Total Flow [kg/h]	117160	117160	117160	24126	24126	3607997	93034
Total Flow [kmol/h]	2454	2454	2454	341	341	50013	2114
Molar vapor fraction [-]	0	0	0.799	0	0	0	1
Molar liquid fraction [-]	0.136	0.136	0.201	1	1	1	0
Molar solid fraction [-]	0.864	0.864	0	0	0	0	0
Temperature [°C]	-113	-111	18	161	30	-111	-5
Pressure [bar]	1.01	30	30	30	29.9	1.01	30
Density [kg/m^3]	1305	1303	91.70	413	619	742	81.99

Stream # in Fig. 2.6	**36**	**37**	**38**
Mole fractions [-]			
CO_2 (S)	0	0	0
CO_2	1	1	1
O_2	0	0	0
N_2	0	0	0
H_2O	0	0	0
Ar	0	0	0
CH_4	0	0	0
C_2H_6	0	0	0
C_3H_8	0	0	0
n-C_4H_{10}	0	0	0
i-C_5H_{12}	0	0	0
CF_4	0	0	0
Total Flow [kg/h]	93034	93034	93034
Total Flow [kmol/h]	2114	2114	2114
Molar vapor fraction [-]	1	0	0
Molar liquid fraction [-]	0	1	1
Molar solid fraction [-]	0	0	0
Temperature [°C]	77	30	38
Pressure [bar]	80	80	110
Density [kg/m^3]	167	629	527

Nomenclature

A	Area [m^2]
AC_{eq}	Equivalent CO_2 Avoided Index [%]
B_z	Mean volumetric heat transfer coefficient of zone z [$kW/m^3 \cdot K$]
c_p	Isobaric heat capacity [J/mol·K]
C_{BM}	Equipment installed cost
C_{OL}	Labor cost [M€]
C_p^0	Equipment purchase cost [$]
CAC	Cost of Avoided CO_2 [€/t_{CO2}]
$(COC)_{CCC}$	Cost of Clinker of the cryogenic carbon capture process [€/t_{clk}]
$(COC)_{ref}$	Cost of Clinker of the reference cement plant [€/t_{clk}]
$(COC)_{ref,CCC}$	Cost of Clinker of the reference cement plant integrated with the cryogenic carbon capture technology [€/t_{clk}]
$e_{clk,eq,CCC}$	CO_2 equivalent emissions of the reference cement plant integrated with the cryogenic carbon capture technology [kg_{CO2}/t_{clk}]
$e_{clk,eq,ref}$	CO_2 equivalent emissions of the reference cement plant [kg_{CO2}/t_{clk}]
$e_{eq,CCC}$	CO_2 equivalent emissions of the cryogenic carbon capture process [kg_{CO2}/t_{clk}]
$\dot{E}_{CCC}$	Power consumption of compressors and pumps [MW]
EPC	Engineering, Procurement and Construction [M€]
$\hat{f}_i^S$	Fugacity of component *i* in solid phase [Pa]
$\hat{f}_i^V$	Fugacity of component *i* in vapor phase [Pa]
F_{BM}	Bare Module factor [-]
F_M	Material factor [-]
F_P	Pressure factor [-]
FOM	Fixed operative costs [M€]
g	Gibbs free energy [J/mol]
h	Enthalpy [J/mol]
ΔH_R^0	Standard enthalpy of reaction [kJ/mol]
i	Interest rate [%]
L	Height of packing bed
$\dot{m}_{CO2\ (S)}$	Mass flowrate of CO_2 in solid phase [kg/s]
MTZ	Height of mass transfer zone [ft]
N_{np}	Number of equipment in the process [-]
N_{OL}	Number of work position per shift [-]
N'_{OL}	Number of operators [-]

$O\&M$	Operating and Maintenance Cost [M€]
P	Absolute pressure [Pa]
P_{CO2}^{subl}	CO_2 sublimation pressure [Pa]
P_S	Shaft power
q	Cumulative heat duty in MHX [MW]
$q_{clk,eq,CCC}$	Equivalent primary energy consumption of the reference cement plant integrated with the cryogenic carbon capture technology [MW_{LHV}/kg_{CO2}]
$q_{clk,eq,ref}$	Equivalent primary energy consumption of the reference cement plant [MW_{LHV}/kg_{CO2}]
$q_{eq,CCC}$	Equivalent primary energy consumption of the cryogenic carbon capture process [MW_{LHV}/kg_{CO2}]
$\dot{Q}_i$	Heat flow rate transferred by stream *i* [kW]
$\dot{Q}_z$	Heat flow rate transferred in zone *z* [kW]
R	Universal gas constant [J/mol·K]
s	Entropy [J/mol]
$SPECCA$	Specific Primary Energy Consumption for CO_2 Avoided [MJ_{LHV}/kg_{CO2}]
T	Absolute temperature [K]
TAC	Total Annualized CAPEX
TDC	Total Direct Cost [M€]
TOC	Total Overnight Cost [M€]
TPC	Total Plant Cost [M€]
u	Internal energy [J/mol]
u_g	Superficial gas velocity [ft/min]
v	Molar volume [m^3/kmol]
v_{CO2}^S	CO_2 solid molar volume [m^3/kmol]
V	Volume [m^3]
V_z	Volume of zone *z* [m^3]
VOM	Variable operative costs [M€]
x_{CO2}^V	Molar fraction of CO_2 in vapor phase [-]

Greek letters

α	Cubic expansion coefficient [K^{-1}]
β_i	Local volumetric heat transfer coefficient of stream *i* [$kW/m^3 \cdot K$]
ε	Relative error [-]
κ	Isothermal compressibility [Pa^{-1}]

π	Reduced pressure [-]
ϕ_{CO2}^{V}	Fugacity coefficient of pure CO_2 in the vapor phase [-]
$\hat{\phi}_{CO2}^{V}$	Fugacity coefficient of CO_2 in vapor vapor mixture [-]
θ	Reduced temperature [-]
γ	Energy penalty [MJ_{el}/kg_{CO2}]

Acronyms

ARC	Absorption Refrigeration Cycle
ASU	Air Separation Unit
BAHX	Brazed Aluminum Heat Exchanger
CaL	Calcium-Looping
CCC	Cryogenic Carbon Capture
CCUS	Carbon Capture Utilization and Storage
CEPCI	Chemical Engineering Plant Cost Index
DEA	Diethnolamine
GWP	Global Warming Potential
IEA	International Energy Agency
IEAGHG	International Energy Agency Greenhouse Gas R&D Program
JS EoS	Jäger and Span Equation of State
KPI	Key Performance Indicator
LNG	Liquefied Natural Gas
MDEA	Methyl diethanolamine
MEA	Monoethanolamine
MHX	Multi-Stream Heat Exchanger
MPS	Medium-Pressure Steam
NETL	National Energy Technology Laboratory
PR EoS	Peng-Robinson Equation of State
PSRK EoS	Predictive Soave-Redlich-Kwong Equation of State
SARC	Swing Adsorption Reactor Cluster
SES	Sustainable Energy Solutions
SRK EoS	Soave-Redlich-Kwong Equation of State
SVE	Solid-Vapor Equilibria
TRL	Technology Readiness Level
VPSA	Vacuum Pressure Swing Adsorption
ZEP	Zero Emission Platform

Bibliographical References

Aaron D. and Tsouris C. (2005). Separation of CO_2 from Flue Gas: a review. *Separation Science and Technology.* 40, 321-348.

Abanades C., Arias B., Lyngfelt A. (2015). Emerging CO_2 capture systems. *International Journal of Greenhouse Gas Control.* 40, 126-166.

Anantharaman R., Berstad D., Cinti G., De Lena E., Gatti M., Gazzani M., Hoppe H., Martìnez I., Monteiro J., Romano M., Roussanaly S., Schols E., Spinelli M., Storset S., Van Os P., Voldsund M. (2017). CEMCAP framework for comparative techno-economic analysis of CO_2 capture from cement plants. *WP3: CEMCAP Framework.* D3.2.

Antzaras A., Papalas T., Heracleous E., Kouris C. (2023). Techno–economic and environmental assessment of CO_2 capture technologies in the cement industry. *Journal of Cleaner Production*. 428, 139330.

Asgharian H., Iov F., Nielsen M. P., Liso V., Burt S., Baxter L. (2025). Cryogenic Carbon Capture Process Combined with Absorption Refrigeration Cycle for Cement Plants – A Danish Case Study. *Separation and Purification Technology*. 353:128419.

Aspen Technology Inc. (2000). Aspen Plus User Guide (Version 10.2). Available at: https://web.ist.utl.pt/ist11038/acad/Aspen/AspUserGuide10.pdf. Last access: 18/09/2024.

Baxter L. (2019). Cryogenic Carbon Capture Development Progress and Field Test Data. Chart™ and Sustainable Energy Solutions. Available at: https://netl.doe.gov/sites/default/files/netl-file/L-Baxter-SES-Cryogenic-Capture.pdf. Last access: 11/09/2024.

Baxter L., Hoeger C., Burt S. (2021). Cryogenic Carbon Capture™ Technoeconomic Analysis. *Proceedings of the 15th Greenhouse Gas Control Technologies Conference 15-18 March 2021.* Available at: https://ssrn.com/abstract=3820158. Last access: 11/09/2024.

Berger A., Hoeger C., Baxter L., Bhown A. (2019). Evaluation of Cryogenic Systems for Post Combustion CO_2 Capture. *SSRN Electronic Journal*. DOI:10.2139/ssrn.3365753.

Cinti G., Anantharaman R., De Lena E., Fu C., Gardarsdottir S., Hoppe H., Jamali A., Romano M., Roussanaly S., Spinelli M., Stallmann O., Voldsund M. (2018). Cost of critical components in CO_2 capture processes. *WP4: Comparative capture process analysis*. D4.4.

Chart Industries Inc. (2023). Brazed Aluminum Heat Exchangers. Available at: https://files.chartindustries.com/Brazed-Aluminum-Heat-Exchangers.pdf. Last access: 18/09/2024.

Cloete S., Giuffrida A., Romano M., Zaabout A. (2020). Economic assessment of the swing adsorption reactor cluster for CO_2 capture from cement production. *Journal of Cleaner Production*. 275, 12024.

d'Amore, F., Romano, M. C., & Bezzo, F. (2021). Optimal design of European supply chains for carbon capture and storage from industrial emission sources including pipe and ship transport. *International Journal of Greenhouse Gas Control*. 109, 103372.

De Guido G., Pellegrini L., Ingrosso S. (2020). Thermodynamic Framework for Cryogenic Carbon Capture. *Computer Aided Chemical Engineering*. 48, 475-480.

De Lena E., Spinelli M., Gatti M., Scaccabarozzi R., Campanari S., Consonni S., Cinti G., Romano M. (2019). Techno-economic analysis of calcium looping processes for low CO_2 emission cement plants. *International Journal of Greenhouse Gas Control*. 82, 244-260.

Eurostat (2024b). *Electricity prices for non-household consumers - bi-annual data (from 2007 onwards)*. Available at: https://doi.org/https://doi.org/10.2908/NRG_PC_205. Last access: 18/09/2024.

Ferrario D., Stendardo S., Verda V., Lanzini A. (2023). Solar-driven calcium looping system for carbon capture in cement plants: Process modelling and energy analysis. *Journal of Cleaner Production*. 394, 136367.

Font-Palma C., Cann D., Udemu C. (2021). Review of Cryogenic Carbon Capture Innovations and Their Potential Applications. *Journal of Carbon Research*. 7(3), 58.

Frankman D., Burt S., Beven E., Parkinson D. (2021). Recent Cryogenic Carbon Capture™ Field Test Results. *SSRN Electronic Journal*. DOI:10.2139/ssrn.3820161.

Gerbelova H., Van Der Speck M., Schakel W. (2017). Feasibility Assessment of CO_2 Capture Retrofitted to an Existing Cement Plant: Post-combustion vs. Oxy-fuel Combustion Technology. *Energy Procedia*. 114, 6141-6149.

Green, D. and Southard, M. (2019). Perry's Chemical Engineers' Handbook (9th ed.). McGraw-Hill Education.

Hewitt G. and Pugh S. (2007). Approximate Design and Costing Methods for Heat Exchangers. *Heat Transfer Engineering*. 28(2), 76-87.

Husebye J., Brunsvold A., Roussanaly S., Zhang X. (2012). Techno Economic Evaluation of Amine based CO_2 Capture: Impact of CO_2 Concentration and Steam Supply. *Energy Procedia*. 23, 381-390.

IEAGHG (2017b). Techno- Economic Evaluation of SMR Based Standalone (Merchant) Hydrogen Plant With CCS. Available at: https://ieaghg.org/publications/techno-economic-evaluation-of-smr-based-standalone-merchant-hydrogen-plant-with-ccs/. Last access: 26/09/2024.

International Energy Agency (2018). Technology Roadmap - Low-Carbon Transition in the Cement Industry. Available at: https://www.iea.org/reports/technology-roadmap-low-carbon-transition-in-the-cement- industry. Last access: 11/09/2024.

International Energy Agency (2021). About CCUS. Available at: https://www.iea.org/reports/about-ccus. Last access: 26/09/2024.

Inveno Engineering Inc. (2017). Best practice no. 16-Knowing the cost of steam. Available at: https://invenoinc.com/file/BestPractices_16.pdf. Last access: 18/09/2024.

IPCC (2022). *Climate Change 2022: Mitigation of Climate Change – Working Group III Contribution to the Sixth Assessment Report*. Available at: https://www.ipcc.ch/report/ar6/wg3/. Last access: 26/09/2024

Jäger A. and Span R. (2012). Equation of State for Solid Carbon Dioxide Based on the Gibbs Free Energy. *Journal of Chemical & Engineering Data*. 57(2), 590-597.

Jaffar M., Brandoni C., Martinez J., Snape C., Kaldis S., Rolfe A., Santos A., Lysiak B., Lappas A., Hewitt N., Huang Y. (2023). Comparative techno-economic analysis of the integration of MEA-based scrubbing and silica PEI adsorbent-based CO_2 capture processes into cement plants. *Journal of Cleaner Production*. 414, 137666.

Jensen M. (2015). Energy Process Enabled by Cryogenic Carbon Capture. *PhD Thesis.* Available at: https://scholarsarchive.byu.edu/etd/5711/. Last access: 11/09/2024.

Kanniche M., Bonnivard R., Jaud P., Valle-Marcos J., Amann J., Bouallou C. (2010). Pre-combustion, post-combustion and oxy-combustion in thermal power plant for CO_2 capture. *Applied Thermal Engineering*. 30, 53-62.

Khaiyum M., Sarker S., Kabir G. (2023). Evaluation of Carbon Emission Factors in the Cement Industry: An Emerging Economy Context. *Sustainability*. 15(21):15407.

Kuramochi T., Ramirez A., Turkenburg W., Faaij A. (2012). Comparative assessment of CO_2 capture technologies for carbon-intensive industrial processes. *Progress in Energy and Combustion Science.* 28, 87-112.

Lindqvist K., Roussanaly S., Anantharaman R. (2014). Multi-stage Membrane Processes for CO_2 Capture from Cement Industry. *Energy Procedia*. 63, 6476-6483.

Liu Z., Jobson M. (1999). The effect of operating pressure on distillation column throughput. *Computers & Chemical Engineering*. 23, S831-S834.

Loh H., Lyons J., White C. (2002). Process Equipment Cost Estimation Final Report. *DOE/NETL-2002/1169*. Available at: https://www.osti.gov/servlets/purl/797810. Last access: 18/09/2024.

Madejski P., Chmiel K., Subramanian N., Kus T. (2022). Methods and Techniques for CO_2 Capture: Review of Potential Solutions and Applications in Modern Energy Technologies. *Energies*. 15(3):887.

Magli F., Spinelli M., Fantini M., Romano M., Gatti M. (2022). Techno-economic optimization and off-design analysis of CO_2 purification units for cement plants with oxyfuel-based CO_2 capture. *International Journal of Greenhouse Gas Control*. 115, 103591.

McKinsey & Company (2008). Carbon Capture and Storage: Assessing the Economics. Available at: https://projects.mcrit.com/foresightlibrary/index.php/megatrens2/environment-sp-1380918679/technologies/337-carbon-capture-and-storage-mckinsey. Last access: 26/09/2024.

Nwaoha C., Beaulieu M., Tontiwachwuthikul P., Gibson M. (2018). Techno-economic analysis of CO_2 capture from a 1.2 million MTPA cement plant using AMP-PZ-MEA blend. *International Journal of Greenhouse Gas Control*. 78, 400-412.

Olajire A. (2010). CO_2 capture and separation technologies for end-of-pipe applications – A review. *Energy*. 35, 2610-2628.

Pachauri R. and Meyer L. (2014). Climate Change 2014: Synthesis Report. Available at: https://www.ipcc.ch/site/assets/uploads/2018/02/SYR_AR5_FINAL_full.pdf. Last access: 18/09/2024.

Perry S., Del Nogal F., Kim J., Smith R. (2008). Optimal Design of Mixed Refrigerant Cycles. *Industrial & Engineering Chemistry Research*. 47(22).

Rubin E., Short C., Booras G., Davison J., Ekstrom C., Matuszewski M., McCoy S. (2013). A proposed methodology for CO_2 capture and storage cost estimates. *International Journal of Greenhouse Gas Control*. 17, 488-503.

Schach M., Oyarzùn B., Schramm H., Schneider R., Rupke J. (2011). Feasibility study of CO_2 capture by anti-sublimation. *Energy Procedia*. 4, 1403-1410.

Scholes C., Ho M., Aguiar A., Wiley D., Stevens G., Kentish S. (2014). Membrane gas separation processes for CO_2 capture from cement kiln flue gas. *International Journal of Greenhouse Gas Control*. 24, 78-86.

Smith J., Van Ness H., Abbott M., Swihart M. (2018). Introduction to Chemical Engineering Thermodynamics (8th ed.). Mc Graw Hill Education.

Song C., Liu Q., Deng S., Li H., Kitamura Y. (2018). Cryogenic-based CO_2 capture technologies: State-of-the-art developments and current challenges. *Renewable and Sustainable Energy Reviews*. 101, 265-278.

Tuinier M. J., Van Sin Annaland M., Kuipers J. (2011). A novel process for cryogenic CO_2 capture using dynamically operated packed beds—An experimental and numerical study. *International Journal of Greenhouse Gas Control.* 5, 694-701.

Turton, R., Bailie, R., Whiting, W., Shaeiwitz, J. (2018). Analysis, Synthesis, and Design of Chemical Processes (5th ed.). Prentice Hall.

U.S. Department of Energy, National Energy Technology Laboratory (2020). Carbon Capture Technology Compendium 2020.

Vatopoulos, K. and Tzimas, E. (2012) Assessment of CO_2 Capture Technologies in Cement Manufacturing Process. *Journal of Cleaner Production*. 32, 251-261.

Voldsund M., Roussanaly S., Gardasrsdottir S., Fu C., Berstad D., Anantharaman R. (2018). CEMCAP comparative techno-economic analysis of CO_2 capture in cement plants. *WP4 Comparative capture process analysis*. D4.6.

Walas, S., Fair J., Penney W., Couper J. (2012). Chemical process equipment: Selection and design (3rd ed.). Butterworth-Heinemann.

Wang C., Soo X., Lee J., Wu W., Tao L., Zhu Q., Bu J. (2024). Advancements in CO_2 capture by absorption and adsorption: A comprehensive review. *Journal of CO_2 Utilization*. 81, 102727.

Wilson P., Lychnos G., Clements A., Michailos S., Font-Palma C., Diego M., Pourkashanian M., Howe J. (2019). Evaluation of the performance and economic viability of a novel low temperature carbon capture process. *International Journal of Greenhouse Gas Control.* 86, 1-9.

Zaman M. (2013). Carbon capture from stationary power generation sources: A review of the current status of the technologies. *Korean Journal of Chemical Engineering*. 30(8).

ZEP (2011c). The Cost of CO_2 Transport. Available at: https://zeroemissionsplatform.eu/wp-content/uploads/CO2-Transport-Report-1.pdf. Last access: 26/09/2024.